Sensors & Diagnostics

CRITICAL REVIEW

View Article Online
View Journal | View Issue

Cite this: *Sens. Diagn.*, 2024, **3**, 745

Aggregation-induced emission-active azines for chemosensing applications: a five-year update

Akhil A. Bhosle, Mainak Banerjee * and Amrita Chatterjee *

Azines are an important class of compounds that display solvent-dependent fluorescence emission depending upon the substituents in the aromatic scaffolds. They are affordable, easy to synthesize, stable, and well-suited for numerous applications. Unlike most other AIE fluorophores, aromatic units of AIE-active azine derivatives are bridged by rotatable N–N bonds rather than C–C bonds. Their derivatives have been widely used in pharmaceuticals, drug delivery, organometallics, optoelectronics, dyes, *etc.*, and most importantly in several sensing applications. This comprehensive review encapsulates the recent developments in the field of AIE-active azine molecules and their applications as chemosensors in the detection of various analytes. The review discusses the different chemosensing strategies involved in the detection of metal ions (Cu^{2+}, Zn^{2+}, Al^{3+}, Fe^{3+}, Cr^{3+}, Hg^{2+}, UO_2^{2+}, *etc.*), anions (F^-, CN^-, ClO^-, $ONOO^-$, HSO_3^-), small molecules (thiols, hydrazine, hydrogen peroxide), and bio-analytes (protamine/heparin, HSA/BSA, neuraminidase, β-lactamase, β-galactosidase, *etc.*) with a focus on the development in the last five years. The review also highlights the advancements in azine-based systems for their use in imaging, supramolecular host–guest recognitions, AIE polymers, COFs/MOFs, *etc.*

Received 4th January 2024,
Accepted 10th April 2024

DOI: 10.1039/d3sd00348e

rsc.li/sensors

1. Introduction

Azines, also known as 2,3-diazabutadienes, are formed by the condensation of carbonyl compounds with hydrazine molecules. They are either symmetrical or unsymmetrical depending upon the carbonyl compounds that combine.[1] These compounds are highly stable, involve easy synthetic protocols, are inexpensive and suitable for diverse applications.[2] Azines with aromatic units bridged by rotatable N–N bonds are one of the few classes of compounds with high fluorescence efficacy. These compounds have been widely used in molecular sensing, particularly for ion sensing, bio-analyte and enzyme detection, pharmaceuticals, dyes, drug delivery, bioimaging, organometallics, optoelectronics, solar cells, light-harvesting systems, *etc.*[3] Polyazines displaying excellent mechanical, thermal, and

Department of Chemistry, BITS-Pilani, K K Birla Goa Campus, NH 17B Bypass Road, Zuarinagar 403726, Goa, India. E-mail: p20190018@goa.bits-pilani.ac.in, mainak@goa.bits-pilani.ac.in, amrita@goa.bits-pilani.ac.in; Tel: +91 832 2580 347, +91 832 2580 320

Akhil A. Bhosle

Akhil A. Bhosle received his B.Sc. and M.Sc. degrees in Chemistry in 2016 and 2018, respectively from Goa University, Goa, India. Later, in January 2019, he joined the Department of Chemistry, BITS Pilani K. K. Birla Goa Campus, Goa, India as a Junior Research Fellow and is now pursuing his doctoral studies under the supervision of Prof. Mainak Banerjee working in the area of mechanochemical synthesis and application of chemosensors.

Mainak Banerjee

Dr. Mainak Banerjee obtained his M.Sc. in Organic Chemistry from University of Calcutta in 1998. He received his Ph.D. degree in 2006 from Jadavpur University, Kolkata India. After two post-doc. stints in South Korea, he started his independent research career in 2009 as an Assistant Professor in the Department of Chemistry at BITS Pilani, K. K. Birla Goa Campus. At present, he is a Professor in the same department. His current research interests include green chemistry, mechanochemistry, supramolecular chemistry, and chemosensors.

semi-conductor properties have been developed from azines as monomers and utilized for electronic and photonic applications.[4]

Conventional fluorophores exhibit strong fluorescence emissions in diluted organic solvents. However, a partial or complete quenching is displayed upon aggregation or in concentrated solutions, reducing their overall efficiency in sensing and bioimaging of the analytes.[5] This effect is called the concentration quenching or the aggregation-caused quenching (ACQ) effect. One of the primary examples of the ACQ effect was studied by Förster and Kasper in 1955, wherein they observed a decrease in the fluorescence emission of pyrene upon increasing the concentration due to the formation of sandwich-shaped excimers and exciplexes (disc-like structures) at the excited state.[6] However, Prof. B. Z. Tang introduced the exact reverse phenomenon in 2001 for a new set of luminophores that fluoresce strongly upon aggregation and could overcome the disadvantages of the ACQ molecules. They coined the term "aggregation-induced emission" to explain the strong emission of propeller-shaped non-planar molecule 1,1′,2,3,4,5-hexaphenyl-1*H*-silole (HPS) by increasing the water fractions in a THF solution.[7] Subsequently, several molecules exhibiting AIE phenomena have been reported in the last two decades and are termed "AIEgens".[8] AIEgens display multiple advantages compared to traditional ACQ molecules in their high fluorescence quantum yield in aggregated states and at higher concentrations, significant Stokes shift, and low cytotoxicity.

AIE-active azine molecules have paved the way for innovative technologies in diverse areas including chemosensing,[3] organic electronic devices,[9] nanomaterials,[10] electro-optical devices,[11] organic functional materials,[12] battery materials,[13] COFs,[14] imaging studies,[15,16] drug delivery,[17] supramolecular chemistry,[18] light-harvesting systems,[19] *etc.* Over the years, there have been many milestone developments in the field of AIE-active azine-based chemosensors (Scheme 1). As a first report, Tong and co-workers reported the synthesis of a range of salicylaldehyde azines which exhibited noteworthy AIE properties depending on the substitutions on the aromatic scaffold.[20] In 2010, Chen *et al.* developed a carboxylic acid functionalized azine derivative that carries a negative charge in basic pH and demonstrated it for the detection of positively charged protamine owing to their electrostatic interactions.[21] In 2014, an azine-derived flavone-based ratiometric probe was reported by Peng *et al.* for the detection of Al^{3+} ions in the solution phase which was one of the early developments in azines as chemosensors for metal ions.[22] Subsequently, Xu *et al.* reported an amphiphilic AIE-active azine, a cationic bola-amphiphile with a salicylaldehyde azine moiety that undergoes a 30-fold emission enhancement upon the addition of γ-cyclodextrin due to the formation of a [2]pseudorotaxane inclusion complex.[18] The azine probe can specifically localize in mitochondria of living cells for fluorescent imaging. In 2016, Liu and co-workers demonstrated an azine-linked luminescent 2D-covalent organic framework incorporating salicylaldehyde with bulky groups as building blocks, which was utilized for Cu^{2+} ion sensing in a selective and sensitive manner.[23] The development of an unsymmetrical azine-derived probe with a naphthalimide moiety was reported by Kumar and co-workers which was utilized for the ratiometric detection of Al^{3+} ions in the solution phase.[24] At a similar time, Zhang & co-workers developed an AIE-active azine-based chemodosimeter by *tert*-butyl dimethylsilyl protection for the sensing of fluoride ions.[25] In 2018, Tang & co-workers reported a tetraphenylethylene-conjugated AIE-active azine by condensation of two TPE units that could recognize Cu^{2+} ions.[26] A year later, Nguyen *et al.* synthesized a water-soluble azine probe to detect Al^{3+} in aqueous solutions.[27] In 2020, Manigandan *et al.* reported a salicylaldehyde-based double azine probe as a highly reliable Fe^{3+} sensor.[28] In the next year, an azine with ESIPT-TICT-AIE triple photophysical characteristics, which is fluorescent both in solution and solid phase featuring orange emission, was reported by our group for the first time and demonstrated in the turn-off sensing of Cu^{2+} ions both in solution and solid phase.[29] Our group further envisaged an AIE active NIR-emissive unsymmetrical azine as a dual-mode-dual-chemodosimeter for the selective and sensitive detection of toxic analytes, N_2H_4 and HSO_3^-.[30] The upcoming section will reflect the advancements in the realm of AIE-active luminogens based on the azine moiety, shedding light on their design, synthesis, optical properties and diverse chemosensing applications. Furthermore, the use of azines in supramolecular sensing, and various azine-derived materials like polymers, MOFs, and COFs in chemosensing applications has been captured in this review. Azines as dual sensors in multi-targeted sensing and imaging are also covered.

Amrita Chatterjee

Dr. Amrita Chatterjee obtained her M.Sc. in Organic Chemistry from the University of Calcutta in 2000 and Ph.D. degree in 2006 from Jadavpur University, Kolkata, India. After post-doc. at POSTECH, Korea from 2006–2009 she joined BITS Pilani, K. K. Birla Goa Campus as an Assistant Professor in 2009. Currently, she is a Professor at the same department. In her independent research career, she developed various molecular sensors (conventional dyes, AIE-based, carbon nanomaterial-based sensors) and focused on greener routes for the synthesis of dyes and sensors.

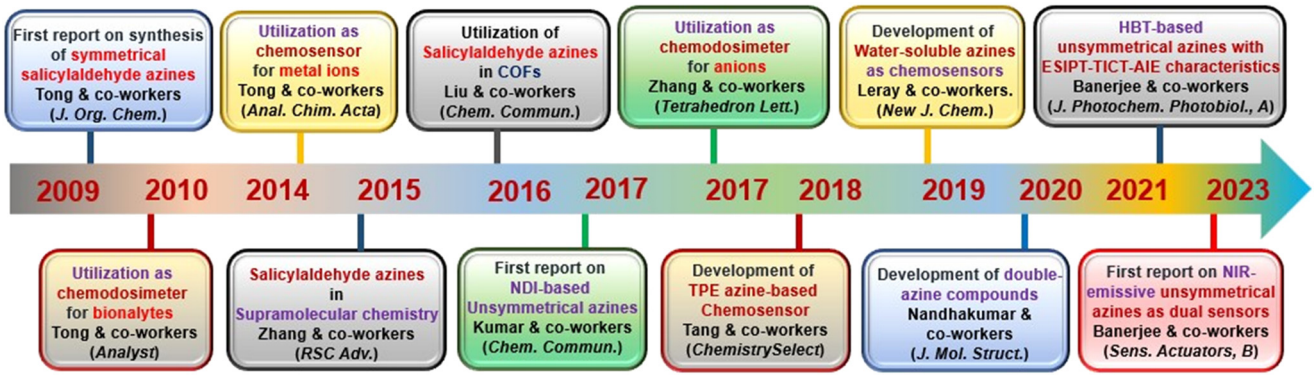

Scheme 1 Key developments in the field of AIE-active azine-based chemosensors.

2. Design and exploration of photophysical properties of azines

Azines, owing to their structural skeleton, display excellent AIE characteristics depending upon the nature of substituents present on the aromatic scaffold. In addition, the presence of different substituents on the aromatic scaffold along the azine linkage induces excellent twisted-intramolecular charge transfer (TICT) characteristics in the scaffold. Similarly, the presence of a hydrogen bond donor functionality such as –OH or $–NH_2$ induces stronger intramolecular hydrogen bonding between the donor

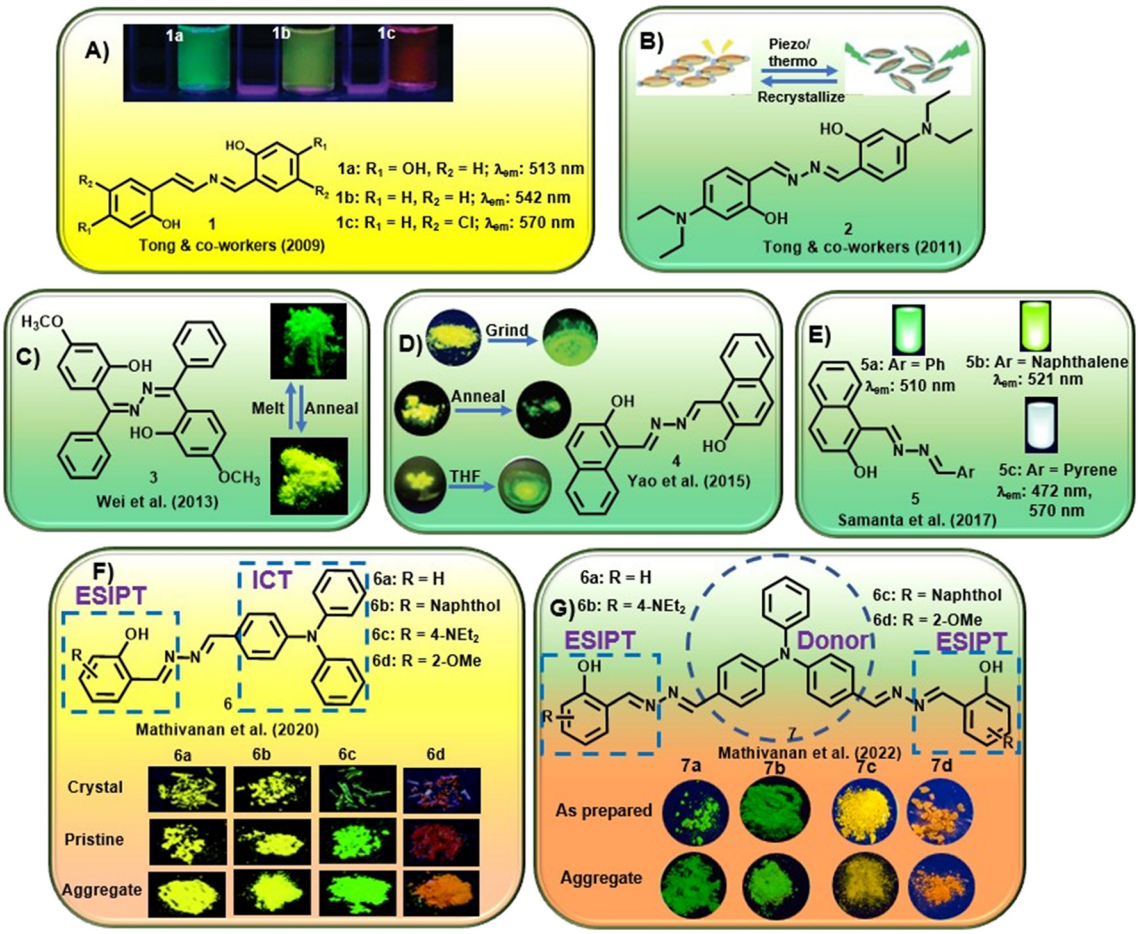

Fig. 1 Selected examples of AIE-active azine compounds studied for their photophysical properties (adapted with permission from: (A) ref. 20. Copyright 2009, American Chemical Society; (B) ref. 31. Copyright 2011, American Chemical Society; (C) ref. 32. Copyright 2013, American Chemical Society; (D) ref. 33. Copyright 2015, Wiley-VCH; (E) ref. 34. Copyright 2017, Royal Society of Chemistry; (F) ref. 35. Copyright 2020, Royal Society of Chemistry; (G) ref. 36. Copyright 2022, Elsevier).

functionality and the –C═N–N═C– linkage resulting in the phenomenon known as excited state intramolecular proton transfer (ESIPT). This section will highlight the design of AIE-active azines for their tunable photophysical properties.

In one of the early attempts, Tong and co-workers synthesized a series of salicylaldehyde-based azine compounds (**1**) that showed appreciable aggregation-induced emission properties [Fig. 1A].[20] These compounds fluoresced weakly in good organic solvents but strongly in poor solvents. Depending on the substituents in the aromatic scaffold, these azines displayed green to orange emission (λ_{max} = 513 nm to 570 nm). The unsubstituted azine, **1b**, displayed yellow emission at λ_{max} 542 nm, whereas when the electron-donating OH group is at the 4-position, azine **1a** showed intense emission at λ_{max} 513 nm. Notably, with the presence of a –Cl substituent at the 5-position, the emission of **1c** showed a red shift to λ_{max} 570 nm. These azines were further explored in hydrazine sensing, which will be discussed later. The same group further envisaged that a planar conjugated core attached to a donor–acceptor (D–A) pair might be a design principle for developing new organic materials with solid luminescence-switching properties. Accordingly, they investigated a symmetrical azine, **2**, for its solid-state fluorescence properties by incorporating a strong electron-donating diethylamino group at the 4-position of the salicylaldehyde azine [Fig. 1B].[31] The azine was responsive to external stimuli like mechanical grinding and temperature. The yellow fluorescence of the compound with emission at 550 nm underwent a significant hypsochromic shift upon grinding or annealing to generate another crystalline form of **2** which emits at 529 nm. The solid-phase transformation with reduced π–π interactions also afforded an amorphous solid that emits at 529 nm with a shoulder peak at 550 nm with intense green fluorescence. The presence of the donor diethylamino group and the acceptor azine moiety functions as a push–pull system and is crucial for solid-state fluorescence-switching. The azines with such push–pull groups could potentially be used in new pressure/thermo-sensing devices. In their continuous study, the authors further synthesized a conformationally flexible symmetrical azine, **3**, by condensing hydrazine with (2-hydroxy-4-methoxyphenyl) (phenyl)-methanone [Fig. 1C].[32] They studied its ESIPT fluorescence changes with respect to the two different polymorphs, green and yellowish green fluorescence, respectively. It was observed that the green emitting polymorph, when annealed at 231 °C for 1 h, induced the phenyl units to stray from their energetically preferred vertical conformation by stronger interactions between them. In contrast, annealing the yellowish-green polymorph eliminated intermolecular connection, restoring the energetically favored conformation. Thus, by alternating annealing/melting procedures, the azine ESIPT fluorescence could be reversibly modified with different emission wavelengths having substantial Stokes shift, high stability and quantum yield.

Yao *et al.* could inculcate mechanochromism in a commercial dye, Pigment Yellow 101. The dye, **4**, was susceptible to mechanical grinding or heat and switched between two structurally distinct polymorphs [Fig. 1D].[33] It was observed that the yellow fluorescence at 543 nm from one polymorph gets converted to the second polymorph with green emission at 530 nm upon grinding in a mortar pestle. In contrast, adding THF or 1,4-dioxane and further grinding after removal of the solvent results in a piezofluorochromic behavior to afford the third polymorph with emission at 566 nm. When heated to 285 °C and annealed, the polymorph converts from yellow to green fluorescence. A reversible transition was obtained after melting and cooling quickly to afford the two original polymorphs.

Samanta *et al.* demonstrated unsymmetrical azines, **5**, to emit white light from a single-component system [Fig. 1E].[34] The naphthol moiety and the azine linkage induced AIE behavior in these compounds and the emission of the azine could be tuned with different water percentages in methanol–water and acetonitrile–water combinations. The introduction of a phenyl (**5a**), naphthyl (**5b**) and pyrene (**5c**) moiety was investigated for linking the AIE scaffold of the naphthyl moiety with dual emission behavior (comprising complementary emission colors) to obtain white light. It was observed that compounds **5a** and **5b** fluoresced strongly at 510 nm and 521 nm, respectively. However, the presence of the pyrene moiety in **5c** afforded a distinct extra emission peak owing to its tendency to form an excimer and resulted in two peaks at 472 and 560 nm. **5c** exhibited variable emission based on the change in the percentage of water and emitted white fluorescence at 70%, 80% and 90% water fractions.

Mathivanan *et al.* synthesized a short series of donor–acceptor unsymmetrical azines, **6**, by condensation of triphenylamine hydrazone and various salicylaldehyde derivatives [Fig. 1F].[35] The azines were designed by utilizing electron-rich triphenylamine as the donor and AIE-active core that also introduces ICT behavior in the scaffold. The imine nitrogen of the azine linkage acts as an electron acceptor and the incorporation of salicylaldehyde units further induces ESIPT behavior with tunable characteristics in the system. The crystal structures confirmed the formation of a supramolecular network from the weak solid-state interactions in addition to the solvent polarity-dependent positive solvatochromic behavior. Electron-donating triphenylamine and diethylamino groups on the scaffold induced pH-dependent emissive properties in the solution. In a continuous effort, the same group further reported a short series of triphenylamine-based symmetrical azines (**7**) involving an acceptor–donor–acceptor type moiety [Fig. 1G].[36] In an attempt to incorporate the ESIPT property in the acceptor–donor–acceptor symmetrical systems, similar to the previous report, an electron-rich triphenylamine unit was utilized as the AIE core as well as the strong donor unit, whereas substituted salicylaldimine units were utilized as electron acceptor groups along with the ESIPT unit. The

azines showed weak fluorescence in solution and significant multi-color emission in the aggregated/solid state, depending on the peripheral substituent owing to the ESIPT and AIE properties. The presence of the methoxy group on the aromatic scaffold was found to exhibit a bathochromic shift and ultimately afford red emission.

Recently, our group discussed the design principle for unsymmetrical azines displaying ESIPT-TICT-AIE triple photophysical properties by combining hydroxybenzothiazole and benzophenone hydrazones [Fig. 2A].[37] The incorporation of a hydroxybenzothiazole (HBT) unit rendered the ESIPT property in the system by keto–enol tautomerism, whereas the azine linkage along with the two phenyl units of hydrazone induces TICT property in the scaffold. The greener and cost-effective mechanochemical method afforded the azine compounds within a short time, avoiding harmful solvents and tedious workup procedures. The orange-to-red emissive azines are highly fluorescent and displayed ESIPT characteristics in organic solvents and AIE characteristics with increased water fractions [Fig. 2A]. The azines revealed solvent-polarity-dependent emission intensities and wavelength shifts based on luminophore aggregation with the maximum emission at 90–93% water fractions in most cases. Incorporating an electron-donating group at the diphenyl methylene unit facilitates electron donation from the donor to the acceptor unit, and a noticeable red shift is observed with the highest red-emission up to 680 nm (**8a–d**). Similarly, the presence of an EWG at the donor moiety lowered the emission wavelength (**8b**). The azines exhibited high quantum yields in different solvents and showed high fluorescence emission in the solid state as well. The molecules displayed a D_1–A–D_2 (or D–π–A) character due to the presence of an EDG (or EWG) at the HBT unit and electron shift from the electron-rich donor diphenyl

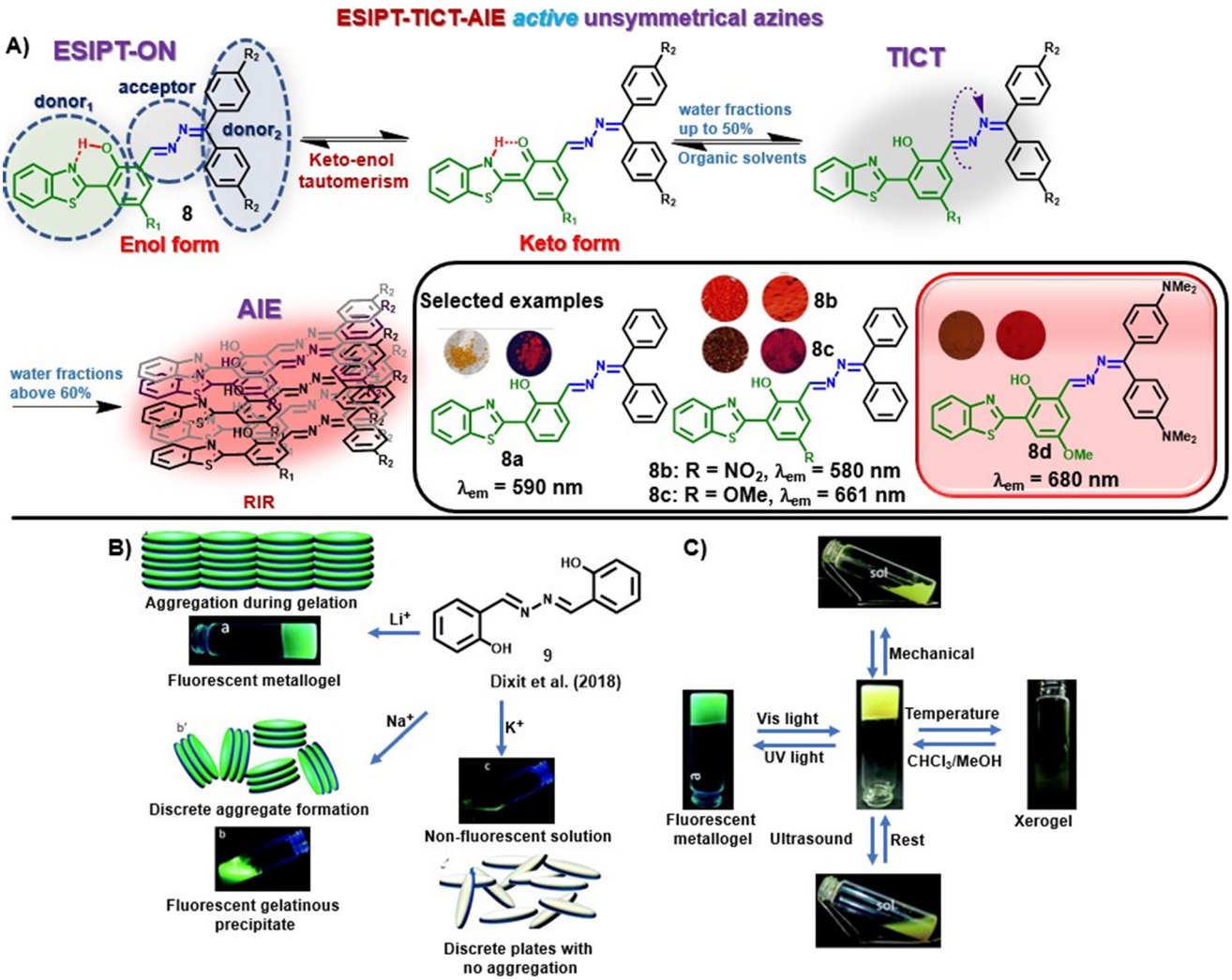

Fig. 2 (A) HBT-based unsymmetrical azine dyes (**8**) having ESIPT-TICT-AIE triple photophysical characteristics (adapted with permission from: ref. 37. Copyright 2023, Wiley-VCH); (B) change in the response of **9** towards LiOH, NaOH, and KOH and their possible molecular arrangement; (C) multi-stimuli responses shown by the metallogel under UV irradiation, ultrasound, mechanical stress and temperature change (images B and C are adapted with permission from ref. 38. Copyright 2018, Royal Society of Chemistry).

Table 1 The collection of azine-based probes and the sensing mechanism, the limit of detection, and applications

Sr. no.	Probe	Analyte	Mechanism/strategy	λ_{ab} / λ_{em} ($\Delta\lambda$)	Solvent system	LOD	Remark	Ref.
1	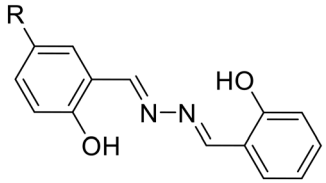 **10a**, R = H **10b**, R = Cl Zhou *et al.* (2018)	Cu^{2+}	Turn-off/complexation (**10** : Cu^{2+} = 1 : 1)	**10a**: 400 nm 552 nm (152 nm) **10b**: 400 nm 536 nm (136 nm)	Phosphate buffer–ACN (9 : 1 v/v, 10 mM, pH 7.4)	**10a**: 0.15 μM **10b**: 0.1 μM	Fluorescence retrieval with S^{2-}	46
2	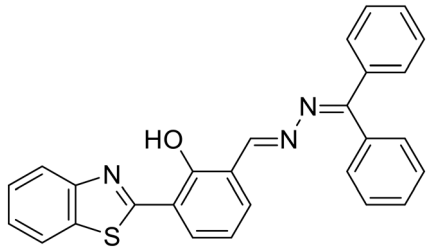 **8a**, Bhosle *et al.* (2021)	Cu^{2+}	Turn-off/complexation (**8a** : Cu^{2+} = 2 : 1)	373 nm 590 nm (217 nm)	H_2O–DMF (9 : 1 v/v)	0.005 μM	Fluorescence retrieval with AA	29
3	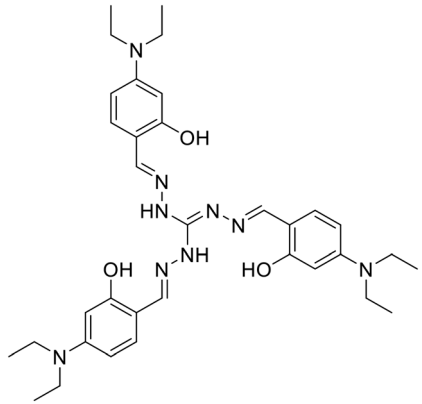 **11**, Tharmalingam *et al.* (2019)	Cu^{2+}	Turn-off/complexation (**11** : Cu^{2+} = 1 : 3)	430 nm 470 nm (40 nm)	ACN–Tris·HCl buffer (9 : 1 v/v, 10 mM, pH 7.2)	0.23 μM	Fluorescence retrieval with S^{2-} Application in solid-phase detection	47

Table 1 *(continued)*

Sr. no.	Probe	Analyte	Mechanism/strategy	λ_{ab} / λ_{em} ($\Delta\lambda$)	Solvent system	LOD	Remark	Ref.
4	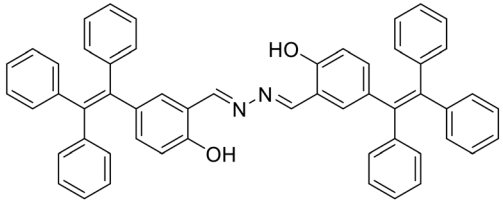 **12**, Zhao *et al.* (2018)	Cu^{2+}	Turn-off/complexation (**12**:Cu^{2+} = 2:1)	380 nm / 581 nm (201 nm)	H_2O–THF (9:1 v/v)	0.03 μM	Fluorescence retrieval with cysteine	26
5	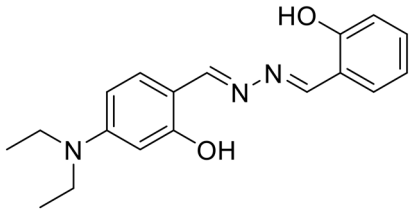 **13**, Tiwari *et al.* (2018)	Cu^{2+}	Turn-off/complexation (**13**:Cu^{2+} = 1:1)	406 nm / 537 nm (131 nm)	EtOH–HEPES buffer (1:1 v/v, 10 mM, pH = 7.4)	0.34 μM	Fluorescence retrieval with PO_4^{3-}, HPO_4^{2-}, $H_2PO_4^-$	48
6	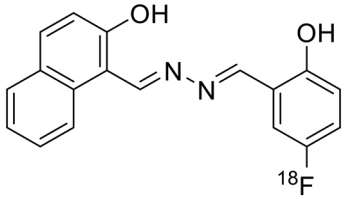 **14**, Ye *et al.* (2021)	Cu^{2+}	Turn-off/complexation (**14**:Cu^{2+} = 1:1)	400 nm / 515 nm (115 nm)	THF–HEPES buffer (1:19 v/v, 20 mM, pH 7.4)	0.16 μM	Fluorescence retrieval with S^{2-}	49
7	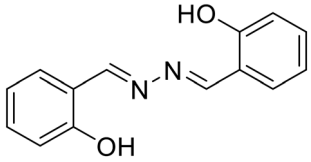 **10a**, Liu *et al.* (2022)	Cu^{2+}	Turn-off/complexation (**10a**:Cu^{2+} = 1:2)	350 nm / 544 nm (194 nm)	H_2O–ACN (9:1 v/v)	0.57 μM	—	50

Table 1 *(continued)*

Sr. no.	Probe	Analyte	Mechanism/strategy	λ_{ab} / λ_{em} ($\Delta\lambda$)	Solvent system	LOD	Remark	Ref.
8	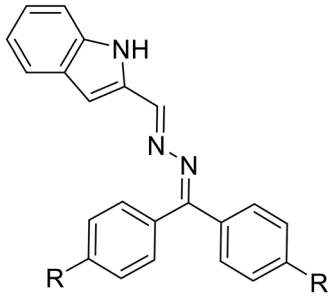 **15a**, R = H	Cu^{2+}	Turn-on/complexation (**15**:Cu^{2+} = 1:1)	350 nm	CAN	**15a:** 0.0008 μM	Fluorescence turn-on response toward CN^-	51
	15b, R = Me			510 nm		**15b:** 0.0013 μM		
	15c, R = F Kumarasamy *et al.* (2022)			(160 nm)		**15c:** 0.0013 μM		
9	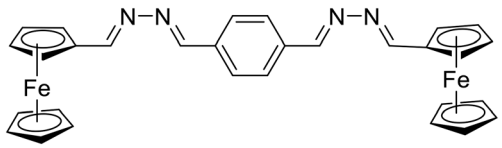 **16**, Sharifi *et al.* (2023)	Cu^{2+}	Turn-on/complexation (**16**:Cu^{2+} = 1:1)	335 nm 671 nm (336 nm)	H_2O–ACN (1:4 v/v)	4.2 μM	—	52
10	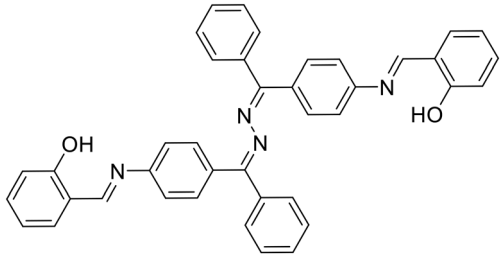 **17**, Kumar *et al.* (2018)	Al^{3+}	Turn-on/complexation (**17**:Al^{3+} = 1:1)	335 nm 490 nm (155 nm)	MeOH	0.27 μM	Application in solid-phase detection	53
11	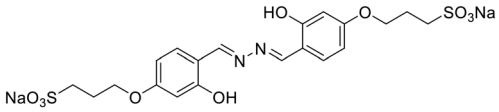 **18**, Nguyen *et al.* (2019)	Al^{3+}	Turn-on/complexation (**18**:Al^{3+} = 1:1)	390 nm 511 nm (121 nm)	HEPES buffer (10 mM, pH 7)	0.153 μM	Application in microfluidic detection	27

Table 1 *(continued)*

Sr. no.	Probe	Analyte	Mechanism/strategy	λ_{ab} / λ_{em} ($\Delta\lambda$)	Solvent system	LOD	Remark	Ref.
12	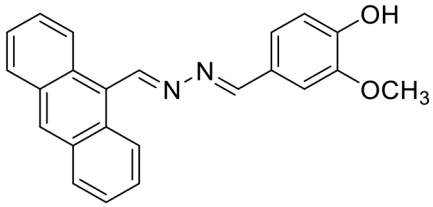 **19**, Khanra *et al.* (2020)	Al^{3+}	Turn-on/complexation (**19**:Al^{3+} = 1:1)	326 nm 400 nm (74 nm)	SDS media (0.1 M HEPES, pH 7.4)	0.0628 μM	—	54
13	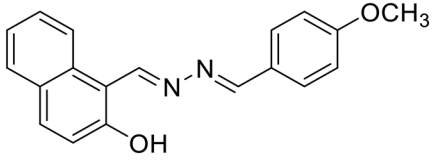 **20**, Khanra *et al.* (2019)	Zn^{2+}	Turn-on/complexation (**20**:Zn^{2+} = 1:1)	400 nm 495 nm (95 nm)	DMSO–bis-Tris buffer (1:1 v/v, pH 7.4)	0.0335 μM	—	55
14	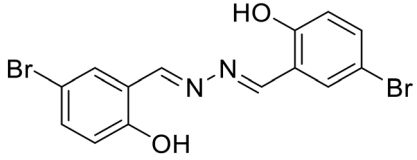 **21**, Das *et al.* (2021)	Zn^{2+}	Turn-on/complexation (**21**:Zn^{2+} = 1:2)	410 nm 532 nm (122 nm)	DMSO–HEPES buffer (9:1 v/v, pH 7.2)	2.18 μM	Fluorescence quenching with picric acid Application in logic gates	56
15	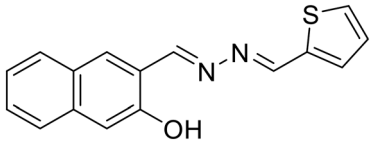 **22**, Musikavanhu *et al.* (2022)	Cr^{3+}	Turn-off/complexation (**22**:Cr^{3+} = 1:1)	408 nm 526 nm (118 nm)	0.2 M HEPES buffer, pH 7.2	0.041 μM	Application in solid-phase detection	57
16	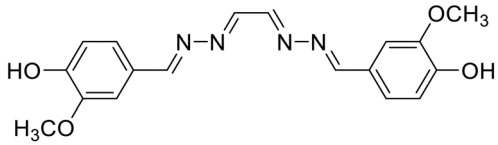 **23**, Manigandan *et al.* (2020)	Fe^{3+}	Turn-off/complexation (**23**:Fe^{3+} = 1:1)	377 nm 423 nm (46 nm)	H_2O–DMF (1:1 v/v)	0.077 μM	Fluorescence retrieval with EDTA	28

Table 1 *(continued)*

Sr. no.	Probe	Analyte	Mechanism/strategy	λ_{ab} / λ_{em} ($\Delta\lambda$)	Solvent system	LOD	Remark	Ref.
17	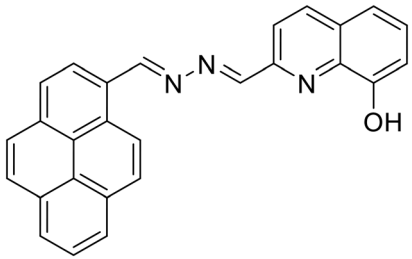 **24**, Mondal *et al.* (2020)	Hg^{2+}	Turn-on/complexation (**24**:Hg^{2+} = 1 : 1)	360 nm 447 nm (87 nm)	H_2O–EtOH (1 : 9 v/v)	0.22 μM	Fluorescence turn-off response towards picric acid	58
18	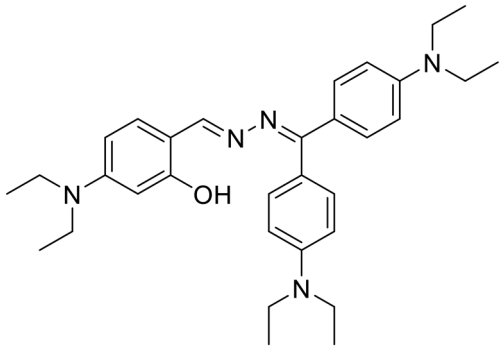 **25**, Tong *et al.* (2020)	Hg^{2+}	Turn-on/complexation	417 nm 558 nm (141 nm)	H_2O–THF (4 : 1 v/v)	7.07 μM	Fluorescence turn-off response towards Cu^{2+}	59
19	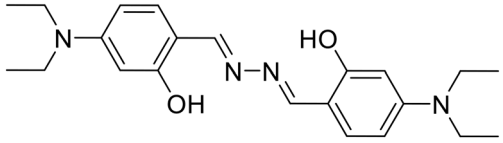 **26**, Ghosh *et al.* (2018)	Mo^{6+}	Ratiometric/complexation (**26**:Mo^{6+} = 1 : 2)	342 nm 501 nm ↑ and 415 nm ↓ (73 nm)	EtOAc–HEPES buffer (10 : 1 v/v, 10 mM, pH 7.4)	0.002 μM	Fluorescence retrieval with S^{2-}	60
20	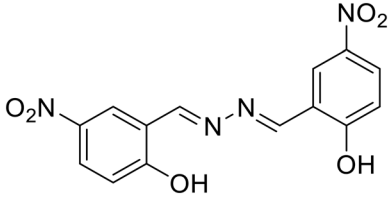 **27**, Pham *et al.* (2019)	UO_2^{2+}	Turn-off/complexation (**27**:UO_2^{2+} = 1 : 1)	365 nm 550 nm (185 nm)	H_2O–ACN (3 : 2 v/v)	0.023 μM	—	61

Table 1 *(continued)*

Sr. no.	Probe	Analyte	Mechanism/strategy	λ_{ab} / λ_{em} ($\Delta\lambda$)	Solvent system	LOD	Remark	Ref.
21	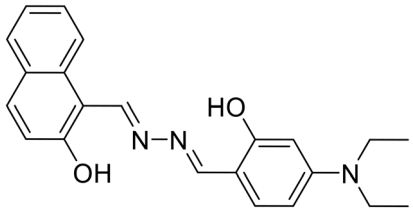 **28**, Yadav *et al.* (2019)	Al^{3+} and Cu^{2+}	Al^{3+}: turn-on, Cu^{2+}: turn-off/complexation (**28**: Al^{3+}/Cu^{2+} = 1 : 1)	434 nm 534 nm (100 nm)	DMSO–HEPES–MeOH (0.1 : 1.9 : 8.0 v/v, pH 7.4)	Al^{3+}: 0.16 μM Cu^{2+}: 0.15 μM	Fluorescence quenching with F^- and retrieval with EDTA Application in solid-phase detection	62
22	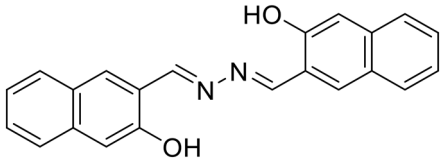 **29**, Sun *et al.* (2023)	Al^{3+} and Cu^{2+}	Turn-off/complexation (**29**: Al^{3+}/Cu^{2+} = 1 : 1)	365 nm 530 nm (165 nm)	Al^{3+}: H_2O–DMSO (1 : 4 v/v) Cu^{2+}: H_2O–DMSO (7 : 3 v/v)	Al^{3+}: 8.47 μM Cu^{2+}: 0.17 μM	Application in solid-phase detection	63
23	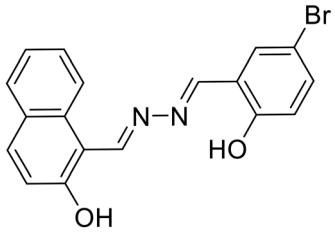 **30**, Das *et al.* (2021)	Al^{3+} and Zn^{2+}	Turn-on/complexation (**30**: Al^{3+}/Zn^{2+} = 1 : 1)	405 nm 532 nm (127 nm)	MeOH–HEPES buffer (9 : 1 v/v, pH 7.2)	Al^{3+}: 9.78 μM Zn^{2+}: 3.65 μM	Application in logic gates	64
24	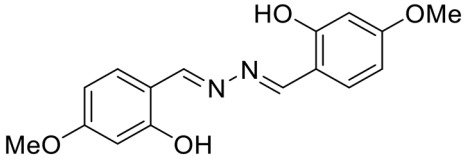 **31**, Dolai *et al.* (2018)	Al^{3+} and Cr^{3+}	Turn-on/complexation (**31**: Al^{3+}/Cr^{3+} = 1 : 1)	360 nm Al^{3+}: 490 nm (130 nm) Cr^{3+}: 427 nm (67 nm)	MeOH–HEPES buffer (4 : 1 v/v, pH 7.4)	Al^{3+}: 4.3 μM Cr^{3+}: 3.4 μM	—	65
25	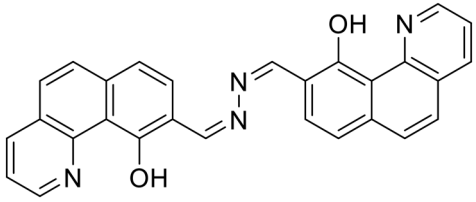 **32**, Sawminathan *et al.* (2021)	Th^{4+} and Fe^{3+}	Turn-on/complexation (**32**: Th^{4+}/Fe^{3+} = 1 : 1)	442 nm 532 nm (90 nm)	H_2O–ACN (4 : 1 v/v)	Th^{4+}: 0.27 μM Fe^{3+}: 5.4 μM	Application in solid-phase detection	66

methylene unit to the acceptor benzothiazole moiety along the azine linkage.

In another study, Dixit *et al.* synthesized a fluorescent metallogel (1% w/v) from a symmetrical azine (**9**) with LiOH in a $CHCl_3$–MeOH mixture [Fig. 2B].[38] The chelation of Li^+ with **9** leads to the inhibition of excited state intramolecular proton transfer (ESIPT) or the origin of fluorescence through chelation-enhanced fluorescence (CHEF), and gelation from aggregation. The metallogel exhibited multi-stimuli responses towards thermal and mechanical stress as well as reswelling properties [Fig. 2C].

3. Azines as chemosensors

Chemosensors for tracing toxic analytes are preferable owing to their convenience, low cost, photostability, sensitivity, and selectivity to analytes. Chemosensors are chemical systems that respond to stimuli *via* fluorescence or color changes. Generally, a recognition site is coupled to a fluorophore, which induces a color or fluorescence change upon interaction with the site-specific analyte and generally involves processes such as ESIPT, PET, ICT, Förster resonance energy transfer (FRET), *etc.* Several chemosensors based on azines have been developed for the selective and sensitive detection of different analytes. The upcoming section will reflect the development of various azine-based chemosensors for the detection of different analytes in the last five years. The section is further classified into: a) metal ion sensors, b) anion sensors, c) small molecules and bioanalyte sensors.

3.1. Metal ion sensors

Metal ions play crucial roles in various essential life processes including body metabolism and regulation of physiological mechanisms.[39] They are categorized as biologically essential metal ions (Ca^{2+}, Fe^{3+}, Zn^{2+} and Cu^{2+}), which must be maintained within an optimal range to ensure their normal biochemical functions, and biologically toxic metal ions (Hg^{2+} and Pb^{2+}) necessitating timely detection. The selective and sensitive detection of these metal ions has become an enduring research objective as any alterations in their concentrations directly impact normal body and physiological functions.[40] In previous years, several AIE-active azines have been designed for the selective detection of metal ions, especially Cu^{2+}, Zn^{2+} and Al^{3+}, mostly by complexation through the azine –N atoms.[22,24,41–45] In general, a 2 : 1 or a 1 : 1 binding between the azine and the metal ion is preferred wherein the analyte binds through the oxygen atom of the attached phenol moiety and an azine nitrogen atom. A snapshot of the azine-based probes, the sensing mechanism, the limit of detection and applications are presented in Table 1.

To further elaborate, in a recent study, Zhou *et al.* utilized salicylaldehyde-derived AIE-active azine, **10**, for the detection of Cu^{2+} ions in a turn-off manner *via* a metal-induced self-assembly mechanism [Fig. 3A and Table 1, entry 1].[46] Upon the addition of 2 equiv. of copper ions, its fluorescence emission at 552 nm was vastly quenched (146-fold). The **10**–Cu^{2+} complex was further employed as an S^{2-} sensor owing to the S^{2-}-induced disassembly of AIE-active azine (**10**). Other metal ions did not complex with **10** and thus they are indifferent to azine, imparting a high selectivity towards Cu^{2+} ions [Fig. 3B]. The images of turn-off response upon the addition of Cu^{2+} ions and subsequent fluorescence revival with S^{2-} were captured under 365 nm UV light and also utilized for acquiring the fluorescence microscopy images of KYSE510 cells [Fig. 3C and D].

We recently demonstrated the use of the benzothiazole-based unsymmetrical azine (**8a**) as a fluorimetric sensor for the turn-off detection of Cu^{2+} ions in solution and solid phase utilizing its ESIPT property [Fig. 3E and Table 1, entry 2].[29] The saturation point was reached at 0.5 equiv. of Cu^{2+} and the stoichiometry of **8a** with Cu^{2+} was established as 2 : 1 from Job's plot, EDX, time-resolved fluorescence measurements, and DFT studies. The sensing was highly selective towards Cu^{2+} ions and no other metal ions displayed any turn-off response [Fig. 3F]. The fluorescence of **8a** can be retrieved by the addition of ascorbic acid (AA) by *in situ* generation of Cu^+ and release of the probe from the complex. Notably, the LOD for **8a** was found to be 0.005 μM, which is about 20 fold lower than Zhou *et al.*'s probe (**10**). The solid-phase sensing ability of the azine was explored using TLC plates which displayed a significant turn-off response at lower concentrations of the Cu^{2+} ions in a selective manner [Fig. 3G]. We demonstrated its practical applicability in real water samples with a high % recovery.

In another work, Tharmalingam *et al.* developed an AIE–ESIPT active star-shaped azine-based Cu^{2+} sensor (**11**) from a triaminoguanidine precursor [Fig. 3H and Table 1, entry 3].[47] Its aggregation-enhanced emissive feature was exhibited in the water–ACN mixture showing an emission maximum at 470 nm. The probe, **11**, displayed solvent-dependent dual emission in nonpolar and polar protic solvents, suggesting excited state ICT-coupled ESIPT characteristics. In this case, a 1 : 3 binding stoichiometry was observed between **11** and Cu^{2+} owing to the presence of three binding sites available in the structural scatffold of the chemosensor [Fig. 3H]. The azine derivative, **11**, exhibited a mechanoresponsive behavior wherein the pristine sample was found to weakly fluoresce greenish yellow and the ground sample showed a bathochromic shift with fluorescence shift to intense green when observed under 365 nm UV light as well as with fluorescence microscopy [Fig. 3I]. The addition of Cu^{2+} resulted in a turn-off response which was found to be reversible towards S^{2-} *via* a metal ion displacement method [Fig. 3J and K]. The reversible and selective on–off–on sensing characteristics of **11** toward Cu^{2+} and S^{2-} were effective in the construction of an IMPLICATION logic gate [Fig. 3L and M]. The probe could also be utilized as an on-site detection tool for the paper-strip-based reversible sensing of Cu^{2+} and S^{2-} ions [Fig. 3N].

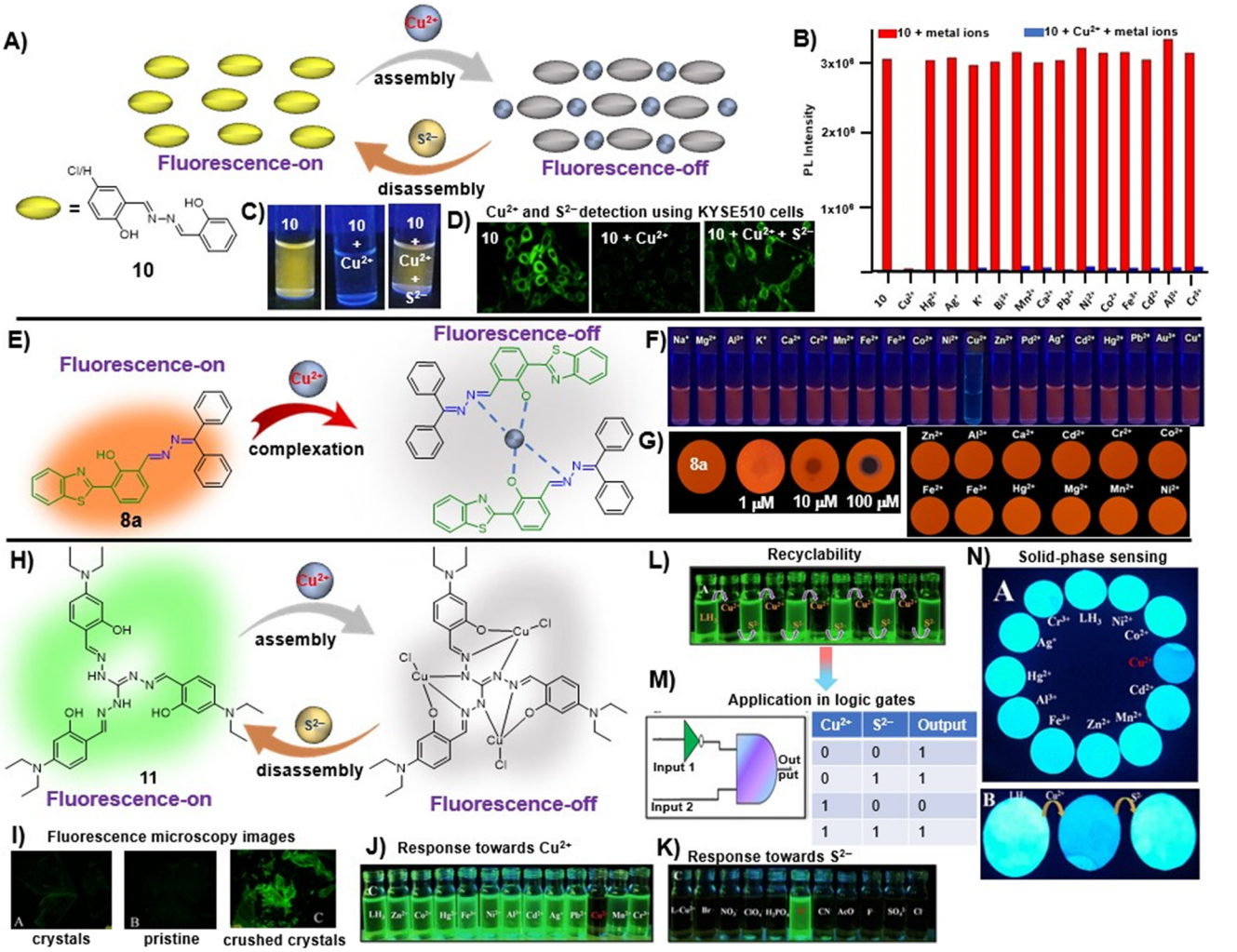

Cu2+	S2−	Output
0	0	1
0	1	1
1	0	0
1	1	1

Fig. 3 (A) Salicylaldehyde-based azine, **10**, as a turn-off chemosensor for Cu^{2+} ions showing 1 : 1 binding stoichiometry and fluorescence retrieval upon the addition of sulfide ions; (B) competitive selectivity of **10** towards different metal ions; (C) images of **10** captured upon the addition of Cu^{2+} ions and S^{2-} under 365 nm UV light depicting visual fluorescence changes; (D) the change in fluorescence microscopy images of KYSE510 cells consisting of **10** after incubation with Cu^{2+} and Cu^{2+} + S^{2-} (images B–D are adapted with permission from ref. 46. Copyright 2018, Elsevier); (E) HBT-based unsymmetrical azine (**8a**) as a turn-off chemosensor for Cu^{2+} ions showing 2 : 1 binding stoichiometry; (F) images of **8a** captured upon the addition of Cu^{2+} ions and other metal ions under 365 nm UV light depicting visual fluorescence changes; (G) on-site detection tool for the TLC-strip-based sensing of Cu^{2+} and selectivity of **8a** towards different metal ions (images F and G are adapted with permission from ref. 29. Copyright 2021, Elsevier); (H) triaminoguanidine-based azine, **11**, as a turn-off chemosensor for Cu^{2+} ions showing 3 : 1 binding stoichiometry and fluorescence retrieval upon the addition of S^{2-} ions; (I) mechanoresponsive behavior of **11** showing weak emission in pristine form and intense fluorescence in ground form; selectivity of **11** towards (J) Cu^{2+} ions and (K) the **11**–Cu^{2+} complex towards S^{2-}; (L) the reversible turn-off–on response of **11** towards Cu^{2+} and S^{2-} and (M) its application in the construction of logic gates; (N) on-site detection tool for the paper-strip-based sensing of Cu^{2+} and S^{2-} (images I–N are adapted with permission from ref. 47. Copyright 2019, American Chemical Society).

Among other notable contributions on azine-based sensors for copper ions, Zhao *et al.* reported a tetraphenylethylene-based AIE-active azine-based compound (**12**) by condensation of two TPE units that could recognize Cu^{2+} ions in a turn-off manner [Table 1, entry 4].[26] The introduction of the azine unit as an electron acceptor could inculcate a bathochromic shift from blue (about 465 nm for typical TPE emission) to orange emission (λ_{max} 581 nm). The probe functioned well as a selective copper ion sensor by 1 : 1 complexation and offered an LOD of 0.03 μM. Similarly, Tiwari *et al.*,[48] Ye *et al.*,[49] Liu *et al.*,[50] Kumarasamy *et al.*,[51] and Sharifi *et al.*[52] demonstrated different symmetrical and unsymmetrical azine-based probes (**10a**, **13**–**16**) with emission in the blue to green region for the detection of Cu^{2+} ions [Table 1, entries 5–9].

Kumar *et al.* synthesized a symmetrical azine (**17**) based on benzophenone and studied its application in the detection of Al^{3+} ions [Table 1, entry 10].[53] The probe, **17**, exhibited weak emission in MeOH due to intramolecular rotations and a typical AIE behavior in >70% H_2O–CH_3CN resulting in intense emission. The azine could detect Al^{3+} in a turn-on manner in MeOH with a limit of detection of 0.27 μM, along with a notable colorimetric response. The binding of Al^{3+} with **17** restricted the intramolecular rotation and caused

enhancement in emission. The stoichiometry was studied by mass spectrometry, NMR titration and Job's plot, which suggested a 1 : 1 ratio of **17** : Al^{3+} in the complex. In another study, Nguyen *et al.* synthesized a salicylaldehyde-derived water-soluble azine (**18**) having terminal sulphonate functionalities to detect Al^{3+} in aqueous solutions [Table 1, entry 11].[27] The sulfonate functional groups in the scaffold provide an enhanced water-solubility to the probe. The complexation of Al^{3+} with **18** *via* the azine –N atom and phenolic –OH causes an aggregation-induced emission enhancement (AIEE) at λ_{max} 511 nm leading to the formation of well-defined dendritic structures. **18** displayed high selectivity towards Al^{3+} ions with a moderate detection limit of 0.153 μM. Only a 15% response towards other metal cations such as Zn^{2+} and Pb^{2+} was observed at high concentrations of these analytes indicating selectivity towards Al^{3+} ions. Further, **18** was incorporated into a digital microfluidic sensor chip, resulting in a sub-micromolar portable detection system for water samples contaminated with Al^{3+}. In another study in the similar direction, Khanra *et al.* synthesized 4-(anthracen-9-ylmethylene-hydrazonomethyl)-2-methoxy-phenol (**19**) and utilized it as a turn-on fluorimetric sensor for Al^{3+} detection in sodium dodecyl sulphate (SDS) medium [Table 1, entry 12].[54]

Khanra *et al.* further reported a β-naphthol derived azine-based chemosensor (**20**) for the detection of Zn^{2+} ions at the nano-molar level [Table 1, entry 13].[55] The chelation of Zn^{2+} ions with **20** results in chelation-enhanced fluorescence (CHEF) through inhibition of ESIPT and –C═N– isomerization and an enhanced emission was observed at 495 nm. The probe displayed negligible CHEF in the presence of other metal ions and showed a detection limit as low as 36.16 nM. The Job's plot and mass analysis confirmed a 1 : 1 binding stoichiometry between **20** and Zn^{2+} ions. In contrast, Das *et al.* reported a turn-on fluorescence sensor using a salicylaldehyde derived azine (**21**) for the selective determination of Zn^{2+} in the presence of acetate ions (AcO^-). The probe exhibited very weak fluorescence. Its emission intensity increases at λ_{max} 532 nm in the presence of Zn^{2+} over several other metal ions, and the emission profile is augmented only when AcO^- is present as the counter anion. They proposed that the addition of Zn^{2+} triggers a synergistic effect and results in pronounced fluorescence enhancement attributed to the Zn^{2+} assisted CHEF process, and inhibition of the PET and ESIPT process [Table 1, entry 14].[56] The binding of Zn^{2+} associated with AcO^- ions locks the free rotation around the –C═N– resulting in the suppression of the non-radiative decay process in the excited state giving strong emission.

Musikavanhu *et al.* derived a naphthol-based azine attached with thiophene (**22**) for the purpose of detecting trivalent chromium (Cr^{3+}) [Table 1, entry 15].[57] The turn-off response at λ_{max} 526 nm with a low detection limit of 0.041 μM can be attributed to the fact that Cr^{3+} is a paramagnetic fluorescence quencher having empty d-shells. Also, the ligand-to-metal charge transfer (LMCT) results in chelation-enhanced quenching (CHEQ). Azine **22** was highly selective towards Cr^{3+} as compared to other competing metal ions owing to Pearson's hard and soft acids and bases (HSAB) theory that defines the greater affinity of hard acid, Cr^{3+}, towards the electron donating imine nitrogen than others.

Manigandan *et al.* reported a symmetrical 4-hydroxy-3-methoxybenzaldehyde-derived azine probe (**23**) as a highly reliable Fe^{3+} sensor [Table 1, entry 16].[28] In 1 : 1 DMF–H_2O, the blue emissive azine (λ_{em} 423 nm) exhibits a sensitive fluorescence "turn-off" response towards Fe^{3+} ions with a limit of detection of 0.077 μM. The azine, **23**, displayed high selectivity towards Fe^{3+} ions over other metal ions except for La^{3+} and Fe^{2+} ions which also showed an appreciable decrease in fluorescence intensities. The energy or electron transfer processes leading to the reverse photo-induced electron transfer process and the paramagnetic property of Fe^{3+} ions along with the unfilled d subshell contributed to the fluorescence quenching of **23**.

Recently, Mondal *et al.* developed a pyrene-hydroxyquinoline-based azine (**24**) for selective turn-on detection of toxic Hg^{2+} ions [Table 1, entry 17].[58] In EtOH–H_2O (9 : 1) medium, **24** showed a turn-on response towards Hg^{2+} ions with a detection limit of 0.22 μM. The probe, **24**, is weakly emissive in 9 : 1 EtOH–H_2O medium and upon the addition of Hg^{2+} ions, it undergoes enhancement that is attributed to the CHEF effect owing to metal–ligand complexation which further triggers the aggregation of the complex and the AIEE effect dominates at higher Hg^{2+} concentrations. The DFT studies indicated that probe **24** acts as a tridentate ligand engaging one of the azine –N atoms, the quinoline –N atom and the –OH group to specifically bind to Hg^{2+}. In another study, Tong *et al.* synthesized a series of azine compounds (**25**) and utilized them for the turn-on detection of Hg^{2+} ions [Table 1, entry 18].[59]

Ghosh *et al.* utilized a salicylaldehyde-based weakly fluorescent azine (**26**) for the detection of Mo^{6+} ions in an EtOH–H_2O (9 : 1) medium [Table 1, entry 19].[60] The planar geometry of **26** favors the PET process involving electron transition from imine –N to the conjugated aldehyde moiety and fluoresces weakly at 415 nm. A ratiometric response is observed with a decrease in peak at 415 nm and a simultaneous increase at 501 nm upon the addition of Mo^{6+} ions. The **26** : Mo^{6+} complex restricts the PET process, leading to CHEF. The formation of a 1 : 2 complex between **26** and Mo^{6+} was observed with a detection limit as low as 0.002 μM. The sensor was applied for the measurement of Mo^{6+} in certified steel samples. The selective extraction of Mo^{6+} from a mixture with other common metal ions using **26** was particularly effective.

Similarly, Pham *et al.* developed a highly selective and sensitive azine-based probe (**27**) for the turn-off detection of uranyl ions in an organoaqueous media [Table 1, entry 20].[61] The addition of UO_2^{2+} ions to **27** in 80% water–ACN fractions resulted in a small decrease in fluorescence intensities, whereas at 60% water fractions, a significant fluorescence quenching was noted. Similarly, the addition of UO_2^{2+} ions to

the unsubstituted azine scaffold did not alter the emission to the extent that was possible with the presence of the $-NO_2$ group in **27**. This was attributed to the electron-withdrawing effect of $-NO_2$ groups which stabilize the phenolate form of **27** in solution and the complexation with UO_2^{2+} ions was more efficient. The complexation of **27** with UO_2^{2+} ions destroyed the aggregation of the probe to solubilize the molecules in the solution resulting in a turn-off response with a **27** : UO_2^{2+} complexation stoichiometry of 1 : 1.

Some azine-based probes with dual metal ion detection ability have also been reported. Yadav *et al.* demonstrated an unsymmetrical azine (**28**) derived from 2-hydroxynaphthalene that exhibits viscochromic and mechanochromic properties and detects Al^{3+} and Cu^{2+} ions *via* two different sensing pathways in DMSO : HEPES : MeOH (0.1 : 1.9 : 8.0, v/v, HEPES buffer, pH 7.4) [Table 1, entry 21].[62] At the outset, a fluorescence turn-on and turn-off mechanism having 1 : 1 binding stoichiometries was displayed upon the addition of Al^{3+} and Cu^{2+} with LODs of 0.165 μM and 0.152 μM, respectively. The stable **28** : Al^{3+} complex formation imparts rigidity resulting in the CHEF effect, which subdues the PET process from the –N atom of azine to the large π-conjugation of the naphthalene moiety, thereby affording an increase in fluorescence intensity. Similarly, the turn-off response with Cu^{2+} is owing to the strong paramagnetic property of Cu^{2+} with a partially filled d-shell showing a high affinity for **28** with N or O as coordinating atoms. The binding of Cu^{2+} leads to CHEQ as the excited state of the fluorophore is suppressed by ligand-to-metal charge transfer (LMCT). F^- and $EDTA^{2-}$ ions made **28** reversible for Al^{3+} and Cu^{2+} ions. Similarly, Sun *et al.* synthesized a series of azine derivatives (**29**) which displayed a turn-on response towards Al^{3+} in DMSO–H_2O (4 : 1) and a turn-off response towards Cu^{2+} in DMSO–H_2O (3 : 7) [Table 1, entry 22].[63]

A naphthol-based fluorescent probe, **30**, was demonstrated by Das *et al.* for the distinguishable turn-on detection of Al^{3+} and Zn^{2+} in different solvent systems (Al^{3+} in MeOH–H_2O (9 : 1) and Zn^{2+} in DMSO–H_2O (9 : 1)) [Table 1, entry 23].[64] In the less polar MeOH–H_2O solvent system, Al^{3+} forms a strong complex with the hard oxophilic donor owing to its small size and high charge. At the same time, **30** is more nucleophilic by capturing the acidic O–H proton in the strong polar solvent DMSO–H_2O. Al^{3+} is strongly passivated by DMSO–H_2O compared with Zn^{2+}, thereby making Zn^{2+} readily available for metal complex formation in the highly-polar solvent. In a similar manner, Dolai *et al.* utilized a weakly emissive salicylaldehyde-based azine probe (**31**) for the turn-on detection of Cr^{3+} and Al^{3+} by two distinct outputs [Table 1, entry 24].[65] The addition of Cr^{3+} and Al^{3+} to **31** resulted in fluorescence enhancement at two different wavelengths (427 nm for Cr^{3+} and 490 nm for Al^{3+}) which is attributed to the CHEF effect and the ICT (intermolecular charge transfer) between the metal ions (Al^{3+} and Cr^{3+}) and **31**. This in turn is due to the different radii of the two metal ions as well as the different ionic potentials (electronic charge/radius of ions).

Sawminathan *et al.* presented a dual-emission responsive azine-based chemosensor (**32**) that uses a colorimetric and fluorescence turn-on technique to quickly, sensitively and selectively detect Th^{4+} and Fe^{3+} [Table 1, entry 25].[66] When exposed to Th^{4+}/Fe^{3+}, the non-emissive **32** emits yellow fluorescence and it offers low detection limits of 2.1 nM and 3.3 nM for Th^{4+} and Fe^{3+}, respectively. Initially, **32** is non-emissive due to the PET phenomenon that occurs from the electronegative –N atom to the highest occupied molecular orbital (HOMO) of the excited fluorophore. However, the addition of Th^{4+}/Fe^{3+} results in turn-on response by blocking the PET process. Paper strips were made using **32** and their ability to sense Th^{4+} and Fe^{3+} in the solid phase was demonstrated. As real samples, several water bodies and human serum albumin were used to successfully assess the performance of **32** in detecting Th^{4+}/Fe^{3+} ions.

3.2. Anion sensors

Anions play a vital role in numerous biological functions and are commercially important for industrial processes.[67] For instance, an optimum concentration of fluoride (F^-) ions is important for dental care and bone structure in the human body, whereas its excess intake results in skeletal fluorosis, leading to stiffness and calcification of bones in the body.[68a] An excess of the strong oxidant peroxynitrite ($ONOO^-$) ions in the system damages proteins and DNA which may result in Alzheimer's disease, cancer, neurodegenerative disorders, inflammation, and diabetes.[68b] Cyanide (CN^-) ions are one of the well-known environmental pollutants owing to their high physiological toxicity.[68c] Hypochlorite (ClO^-) accumulation generates oxidative stress and can lead to various neurodegenerative and cardiovascular diseases and cancer.[68d] Bisulfite (HSO_3^-) is a common antioxidant and food preservative, however, excessive exposure can result in tissue damage and allergic reactions.[68e] Hence their selective and sensitive detection has gained considerable attention. In previous years, several azine-based probes with appropriate functionalities have been utilized for the selective detection of a number of anions such as F^-,[25] CN^-,[69–71] and $^tBuO^-$.[72]

Among recent developments, Shen *et al.* synthesized a diphenylphosphinate-protected salicylaldehyde-based azine chemodosimeter (**33**) and utilized it for the detection of peroxynitrite ($ONOO^-$) ions [Fig. 4A and Table 2, entry 1].[73] The $ONOO^-$ ions could cleave the diphenylphosphinate group to afford the green fluorescent salicylaldehyde azine (λ_{max} 520 nm) back in the solution to offer turn-on sensing for $ONOO^-$ ions [Fig. 4A]. The probe, **33**, could detect endogenous $ONOO^-$ ions with high selectivity and excellent sensitivity and demonstrated a low detection limit of 0.08 μM [Fig. 4B]. The probe was further investigated for its ability to image $ONOO^-$ in living cells and it was found that the probe could specifically detect endogenous $ONOO^-$ in HeLa cells [Fig. 4C]. Yuan *et al.* synthesized another azine-based probe (**34**) for the detection of F^- ions by incorporating 2-hydroxy-1-naphthaldehyde and 1,8-naphthalimide [Fig. 4D and Table 2,

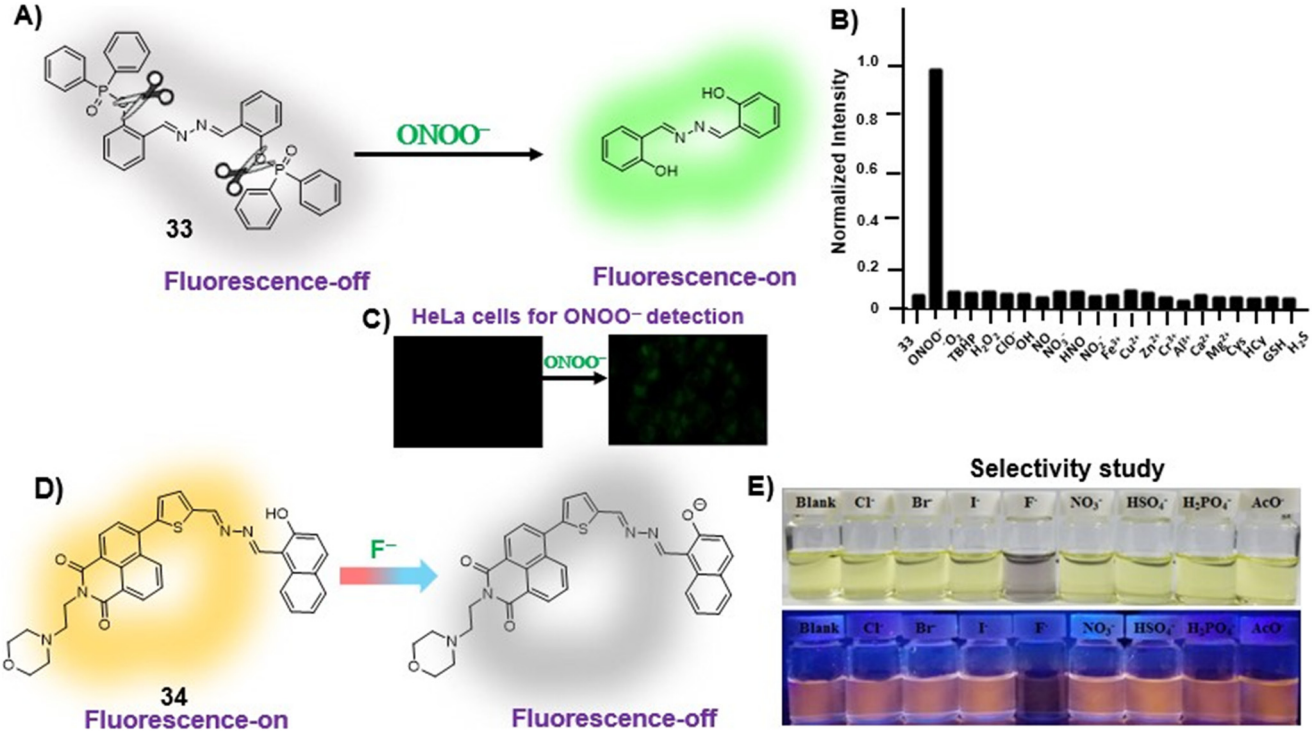

Fig. 4 (A) Diphenylphosphinate modified salicylaldehyde-based azine (**33**) as a turn-on chemodosimeter for $ONOO^-$ ions by cleavage of the diphenylphosphinate group; (B) selectivity of **33** against different analytes depicting high selectivity towards $ONOO^-$ ions; (C) fluorescence microscopy images of HeLa cells in the presence of **33** and $ONOO^-$ ions (images B and C are adapted with permission from ref. 73. Copyright 2019, Elsevier); (D) naphthalimide-based azine (**34**) as a turn-off chemodosimeter for F^- ions by the deprotonation strategy; (E) selectivity studies depicting a change in color from yellow to light purple and fluorescence quenching in the presence of F^- ions (adapted with permission from ref. 74. Copyright 2018, Elsevier).

entry 2].[74] In the presence of F^- ions, **36** results in a color shift from yellow to light purple along with a fluorescence change in a turn-off manner [Fig. 4E]. The ^1H NMR titration revealed that **36** undergoes deprotonation of phenolic –OH *via* a hydrogen-bond interaction between phenolic OH^- and F^- ions. The deprotonation blocks the ESIPT process and tautomerization from the enol form to keto form occurs which induces the PET effect in the system.

Devendhiran *et al.* reported a series of coumarin-based azines (**35**) and utilized them for the selective and sensitive turn-on detection of CN^- ions [Table 2, entry 3].[75] The probe works as a turn-off sensor by nucleophilic addition of the ions across the azine double bond with a detection limit of 0.058 μM. Similarly, Yao *et al.* developed a naphthalene-based unsymmetrical azine (**36**) to detect CN^- in aqueous media *via* a turn-off fluorescence response resulting from the deprotonation of phenolic –OH [Table 2, entry 4].[76] The probe, **36**, recognizes CN^- with good selectivity and sensitivity displaying an LOD of 0.01 μM. Paul *et al.* demonstrated a naphthalene hydrazone-based unsymmetrical azine (**37**) as a turn-on sensor for the detection of CN^- ions [Fig. 5A and Table 2, entry 5].[77] Azine **37** displayed typical AIE characteristics, having weak emission at 503 nm in ACN and the highest emission intensity at 80% water fractions with a bathochromic shift from 503 nm to 537 nm [Fig. 5B]. The probe was utilized for the turn-on detection of CN^- ions in ACN–HEPES buffer. The sensing mechanism is based on the deprotonation by the mild base CN^- to facilitate an extensive delocalization of charge between phenolate $-O^-$ and the aromatic rings in the planar form leading to fluorescence enhancement. They also proposed that the cleavage of the intramolecular hydrogen bonding might stop the ESIPT. The probe showed high sensitivity towards CN^- ions with a limit of detection of 45.4 nM [Fig. 5C] with a high selectivity against most other interfering anions [Fig. 5D]. Azine **37** showed intense emission in the solid state and was therefore utilized for the sensitive detection of trifluoroacetic acid (TFA) vapors *via* fluorescence quenching with an LOD of 1.41 ppm [Fig. 5E]. The protonation-driven destruction of compacted arrangement in the solid state was assumed to be the quenching mechanism of **37**. The turn-off system was further utilized for the reversible acidochromic behavior upon the sequential addition of triethylamine vapors [Fig. 5F]. The probe, **37**, was reversible with TFA and triethylamine (TEA) and the system could easily be recycled several times, demonstrating its potent reusability [Fig. 5G].

Singh *et al.* demonstrated a few azine-based sensors (**38**) for the reversible detection of hypochlorite in aqueous media employing the protonation–deprotonation strategy [Table 2, entry 6].[78] The AIE–ESIPT-active assemblies of salicylaldehyde/indolium-based probes (**38a**) displayed sensitive detection of hypochlorite with a detection limit of

Table 2 Azine-based probes for anion sensing

Sr. no.	Probe	Analyte	Mechanism/strategy	λ_{ab} / λ_{em} ($\Delta\lambda$ nm)	Solvent system	LOD	Remark	Ref.
1	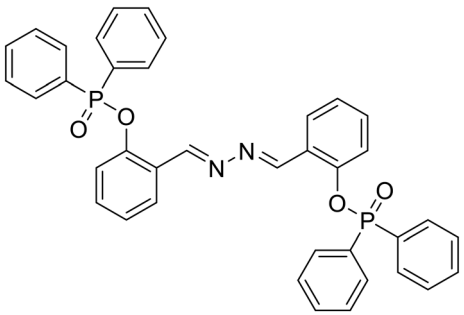 **33**, Shen *et al.* (2019)	$ONOO^-$	Turn-on/diphenyl phosphinate cleavage	403 nm 520 nm (117 nm)	DMSO–PBS buffer (1 : 99 v/v, 50 mM, pH 7.4)	0.08 μM	—	73
2	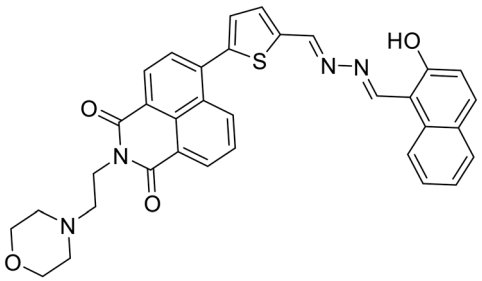 **34**, Yuan *et al.* (2018)	F^-	Turn-off/deprotonation	420 nm 593 nm (173 nm)	THF	0.015 μM	—	74
3	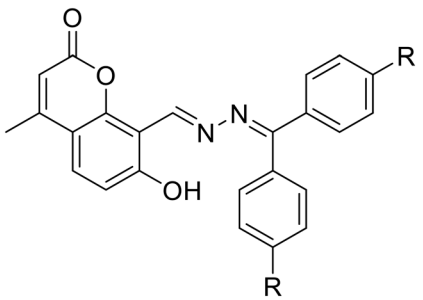 **35a**, R = H **35b**, R = Me **35c**, R = F **35**, Devendhiran *et al.* (2021)	CN^-	Turn-on/nucleophilic addition	320 nm 440 nm (120 nm)	ACN	0.058 μM	—	75
4	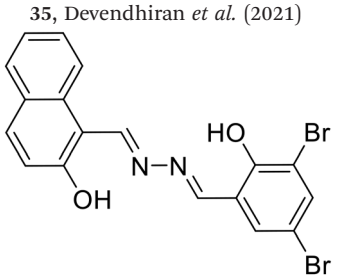 **36**, Yao *et al.* (2022)	CN^-	Turn-off/deprotonation	413 nm 562 nm (149 nm)	H_2O–DMSO (3 : 2 v/v)	0.01 μM	Fluorescence retrieval with H^+ Application in solid-phase detection	76
5	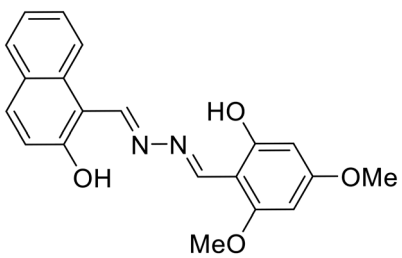	CN^-	Turn-on/deprotonation	365 nm 565 nm (200 nm)	ACN–HEPES buffer (99 : 1 v/v, pH 7.3)	0.045 μM	Solid state fluorescence quenching with TFA vapors and reversible with TEA vapors	77

Table 2 *(continued)*

Sr. no.	Probe	Analyte	Mechanism/strategy	λ_{ab} / λ_{em} ($\Delta\lambda$ nm)	Solvent system	LOD	Remark	Ref.
	37, Paul *et al.* (2023)							
6	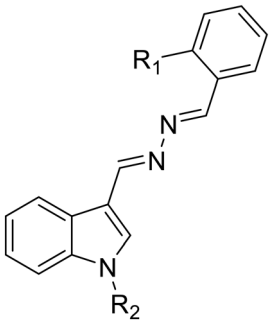 **38a**, $R_1 = R_2 = H$ **38b**, R_1 = OH, $R_2 = H$ **38c**, R_1 = OH, R_2 = Me Singh *et al.* (2020)	ClO^-	Turn-on/deprotonation	350 nm 530 nm (180 nm)	DMSO–PBS buffer (1 : 4 v/v, pH 7.4)	0.05 μM	Application in solid-phase detection	78

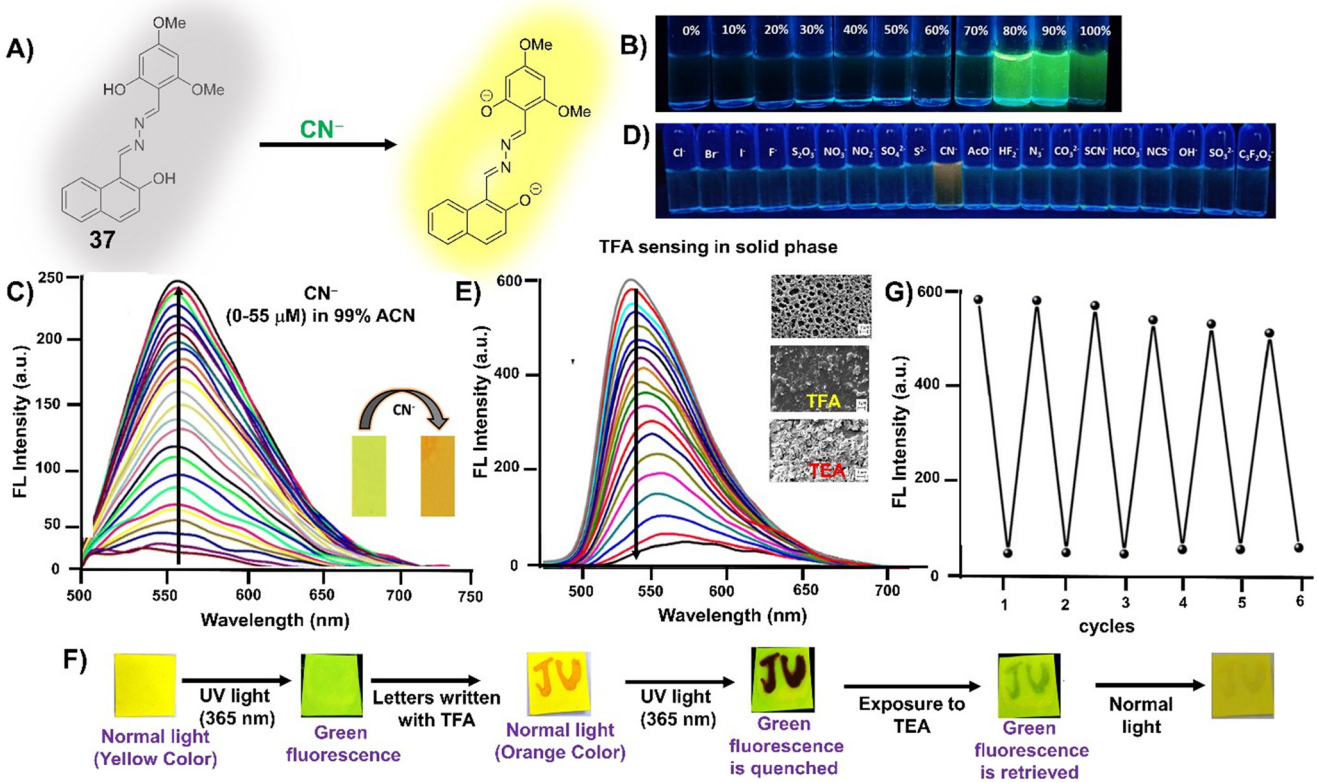

Fig. 5 (A) Naphthalene-based azine (**37**) as a turn-on chemodosimeter for CN^- ions by the deprotonation strategy; (B) AIE behavior exhibited by **37** with the highest intensity at 80% water fractions; (C) turn-on response of **37** upon the addition of CN^- ions in 99% ACN; (D) selectivity of **37** against different analytes; (E) turn-off response of **37** upon the addition of TFA vapors in the solid state; (F) reversibility of the turn-off–on mechanism against addition of TFA followed by TEA; (G) reusability study of **37** against TFA vapors and TEA vapors showing high sensitivity and accuracy even after 6 cycles (adapted with permission from ref. 77. Copyright 2023, Royal Society of Chemistry).

0.052 μM. The highly sensitive response to ClO^- ions was owing to the elevated acidity and the formation of more organized structures following deprotonation. Additionally, the 'dip strip' of **38a** has been used to show the real-time use for 'on-site' solid-phase detection of hypochlorite. Moreover, these assemblies were effectively employed for visualizing

hypochlorite within cells and acted as antioxidants to avert cell death induced by hypochlorite.

3.3. Small molecule and bioanalyte sensors

Some small molecules such as hydrogen peroxide (H_2O_2) and hydrazine (N_2H_4) are crucial for human health and they can contaminate water and soil in higher concentrations. Elevated levels of H_2O_2 in the body are linked to various diseases, including malignant tumors, Parkinson's syndrome, Alzheimer's disease, *etc.*[79a] Meanwhile, excessive utilization of hydrazine results in elevated concentrations in water bodies and soil that readily move into humans through oral, dermal or inhalation routes owing to its volatile nature, leading to significant harm to the lungs, liver, kidneys, central nervous system and respiratory system.[79b] On the other hand, bioanalytes regulate a number of biological functions in the body and are important for the healthy functioning of physiological processes. Among a few important species of interest, protamine is used for the treatment of thrombotic diseases as an anticoagulant and in case of heparin overdosage. Higher concentrations of heparin induce thrombocytopenia, hemorrhages, and hyperkalemia.[79c] β-Lactamase acts as a key biomarker for pathogenic bacteria that show resistance to β-lactam antibiotics by effectively catalyzing the cleavage of the amide group in the antibiotics.[79d] Influenza virus proteins such as neuraminidase (NA) play a vital role in influenza virus infection and replication in host cells.[79e] Accurate quantification of biological thiols, including cysteine (Cys) and glutathione (GSH), is crucial as their aberrant levels are associated with various conditions such as cancer, liver damage, slow growth and skin lesions.[79f] In the past, several azine-based probes with appropriate functionalities have been utilized for the selective detection of bioanalytes and neutral molecules such as Cys,[80] protamine,[21] heparin,[81] hydrophobic proteins (casein) or proteins composed of hydrophobic pockets (bovine serum albumin (BSA) and human serum albumin (HSA)),[82,83] egg albumin,[84] brown adipose cells,[85] β-galactosidase,[86] pyrophosphate,[87] pH indicators,[88] *etc.* which is comprehensively reviewed by Kagatikar *et al.*[3]

In recent times, Sathiyaraj *et al.* synthesized a short series of *N*,*N*-dimethylaminobenzaldehyde-based symmetrical azines (**39**) having electron-donating amino substituents as the recognition sites for the detection of nitro explosive, picric acid [Table 3, entry 1].[89] The donor–π–donor probe displayed high selectivity in an aggregated form which arises from the substituents at the amine group. Notably, picric acid enhanced the fluorescence of the azine monomers in pure THF but quenched the same in the THF–water mixture. In THF, picric acid forms a hydrogen bonding network with one of the amine nitrogen atoms, resulting in an electron-accepting group instead of an electron donor. Further, the fluorescence quenching with PA was attributed to the inner filter effect and the disturbance of aggregates by the hydrogen bonding interaction between the nitrogen of PA and *N*,*N*-dialkylamino group. Similarly, our group utilized the red-emissive HBT-based unsymmetrical dyes, **8d**, for the detection of nitroaromatic compounds (NACs) [Table 3, entry 2].[37] The electron-deficient NACs in particular, picric acid, undergo noncovalent interactions with electron-rich azines resulting in the turn-off detection of NACs [Fig. 6A]. The disruption in the aggregation is due to the intercalation of nitroaromatics in an ordered array of **8** by more favorable π–π interactions. The red-emissive azine with the highest emission maxima, **8d**, exhibited a turn-off response towards PA in 1 : 19 v/v DMF–H_2O with a limit of detection of 0.09 μM. The probe, **8d**, displayed variable responses to other NACs such as 2,4-dinitro-chlorobenzene and 4-nitrotoluene and was non-responsive against other aromatic compounds with no or insignificant turn-off response [Fig. 6B].

Our group further utilized one of the benzothiazole-derived unsymmetrical azines with a *p*-Cl substituent (**8**) and protected it with a benzyl boronic acid group as the recognition unit for the selective detection of H_2O_2 ions to afford a turn-on chemodosimeter [Fig. 6C and Table 3, entry 3].[90] H_2O_2 spontaneously cleaves the benzyl boronic acid group of the chemodosimeter (**40**) in 1% DMSO in PBS (10 mM, pH 7.4) medium to produce its precursor **8**, which emits intense orange AIE [Fig. 6D]. The probe was non-responsive to other ROS, cations, anions, oxidizing, and reducing agents. The high sensitivity of **40** towards H_2O_2 is attributed to a low limit of detection (LOD) of 3.9 × 10^{-8} M (1.3 ppb). The practical utility of **40** in H_2O_2 detection was demonstrated by spiking H_2O_2 in water samples collected from local water bodies and in blood serum. Azine **40** was successfully demonstrated in solid-phase detection of H_2O_2 using TLC plates as the platform, a smartphone for image-capturing, and ImageJ analysis for a practical demonstration of the on-site quantitation of H_2O_2 [Fig. 6E]. The probe, **40**, could efficiently detect intracellular H_2O_2, as shown by imaging in live HeLa cells [Fig. 6F].

Song *et al.* developed a salicylaldehyde-based azine chemodosimeter, **41**, protected with a dinitrobenzene sulphonyl group for the detection of Cys/Hcy in a turn-on manner [Table 3, entry 4].[91] The addition of Cys/Hcy to the probe solution resulted in the cleavage of the 2,4-dinitro benzenesulfonate group of **41** to afford the turn-on response. The probe, **41**, displayed a significant Stokes shift (148 nm), low cytotoxicity, and good photostability. It was further utilized as a portable kit for the on-site inspection of more than ten micro samples simultaneously which might successfully reduce the development of false positives and visual errors. In addition, it was also demonstrated for cell imaging using PC12 cells, establishing its potential in the detection of Cys/Hcy in live cells.

Azinphos-methyl (Guthion) is a broad spectrum organophosphate (OPP) insecticide and an acetylcholinesterase inhibitor. It is classified as an extremely

Table 3 Azine-based probes for bio-analyte and small molecule sensing

Sr. no.	Probe	Analyte	Mechanism/strategy	λ_{ab} / λ_{em} ($\Delta\lambda$ nm)	Solvent system	LOD	Remark	Ref.
1	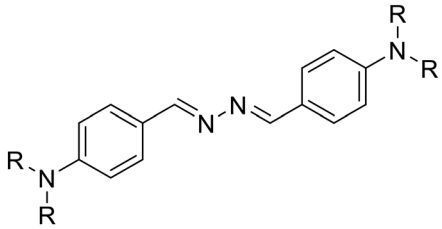 **39a**, R = Me **39b**, R = Et **39c**, R = Pr **39d**, R = Ph Sathiyaraj *et al.* (2020)	Picric acid	THF: turn-on, hydrogen bonding	THF: 415 nm 570 nm (155 nm)	THF or H_2O–THF (7 : 3 v/v)	THF: 26 μM	—	89
			H_2O–THF: turn-off, protonation at azine N	H_2O–THF: 443 nm 490 nm (47 nm)		H_2O–THF: 38 μM		
2	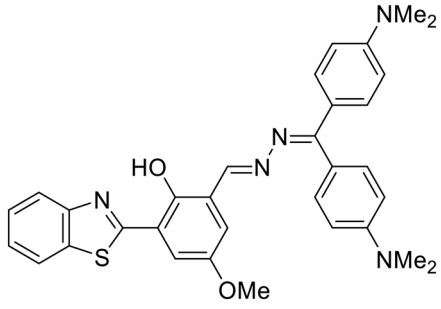 **8d**, Bhosle *et al.* (2023)	NACs	Turn-off/disruption of AIE property by intercalation of NACs	398 nm 675 nm (277 nm)	H_2O–DMF (19 : 1 v/v)	0.09 μM	Application in solid-phase detection	37
3	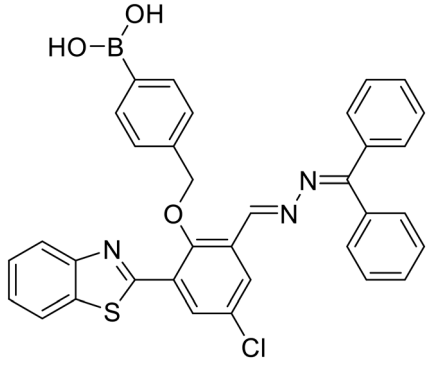 **40**, Bhosle *et al.* (2022)	H_2O_2	Turn-on/benzyl boronic acid cleavage	384 nm 617 nm (233 nm)	DMSO–PBS buffer (0.1 : 9.9 v/v, 10 mM, pH 7.4)	0.039 μM	Application in solid-phase detection	90

Table 3 *(continued)*

Sr. no.	Probe	Analyte	Mechanism/strategy	λ_{ab} / λ_{em} ($\Delta\lambda$ nm)	Solvent system	LOD	Remark	Ref.
4	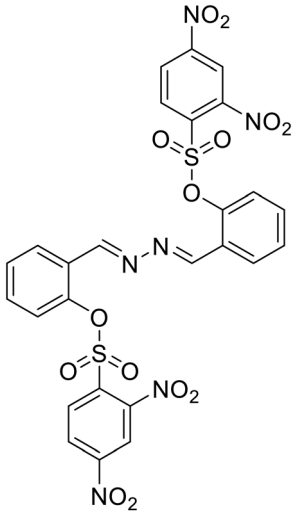 **41**, Song *et al.* (2018)	Cys	Turn-on/dinitro benzene sulphonyl cleavage	405 nm / 547 nm (142 nm)	DMSO–PBS buffer (1 : 9 v/v, 10 mM, pH 7.4)	2.84 μM	Application in solid-phase detection	91
5	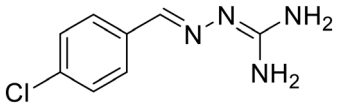 **42**, Bhattu *et al.* (2023)	Azinphos-methyl	Turn-on/H-bonding interactions	275 nm / 355 nm (80 nm)	H_2O	7.4 μM	—	92
6	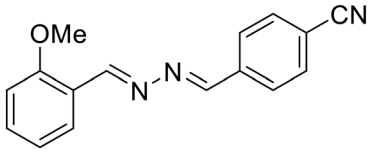 **43**, Thiagarajan and co-workers (2021)	Diethylchlorophosphate (DCP)	Turn-on/ACN: nucleophilic substitution at azine N	ACN: 373 nm / 495 nm (122 nm)	ACN or 80% H_2O–ACN (4 : 1 v/v)	ACN: 0.0099 μM	—	93
			ACN–H_2O: protonation at azine N	ACN–H_2O: 269 nm / 432 nm (163 nm)		ACN : H_2O: 0.068 μM		
7	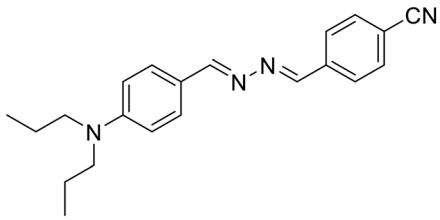 **44**, Sathiyaraj *et al.* (2020)	Diethylchlorophosphate (DCP)	Turn-on/THF: nucleophilic substitution at azine N	THF: 440 nm / 513 nm (73 nm)	THF or H_2O: THF (7 : 3 v/v)	THF: 0.2 μM	—	94
			THF : H_2O: protonation at azine N	THF : H_2O: 368 nm / 570 nm (202 nm)		THF : H_2O: 106 μM		
8		Alkaline phosphatase (ALP)	Turn-on/phosphate cleavage	356 nm / 536 nm	50 mM Tris buffer, pH 9	0.012 U L^{-1}	—	95

Table 3 *(continued)*

Sr. no.	Probe	Analyte	Mechanism/strategy	λ_{ab} / λ_{em} ($\Delta\lambda$ nm)	Solvent system	LOD	Remark	Ref.
				(180 nm)				
	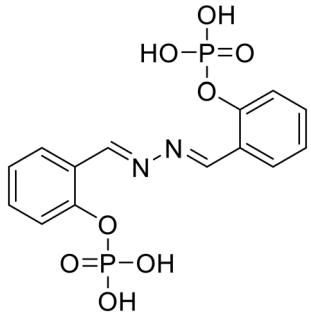 **45**, He *et al.* (2020)							
9	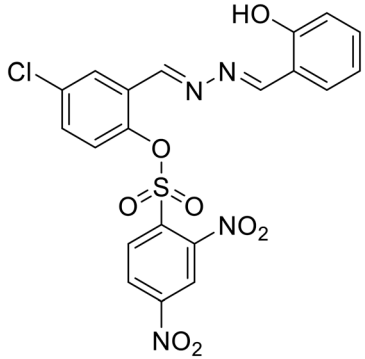 **46**, Tong and co-workers (2018)	β-Lactamase	Turn-on/dinitro benzene sulphonyl cleavage	400 nm 558 nm (158 nm)	PBS buffer (10 mM, pH 7.4)	0.5 mU mL^{-1}	NA	96
10	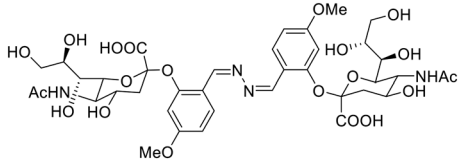 **47**, Chang *et al.* (2022)	Neuraminidase (NA)	Turn-on/sialic acid cleavage	387 nm 524 nm (137 nm)	10 mM PBS buffer (pH 7.4)	0.024 U mL^{-1}	—	97

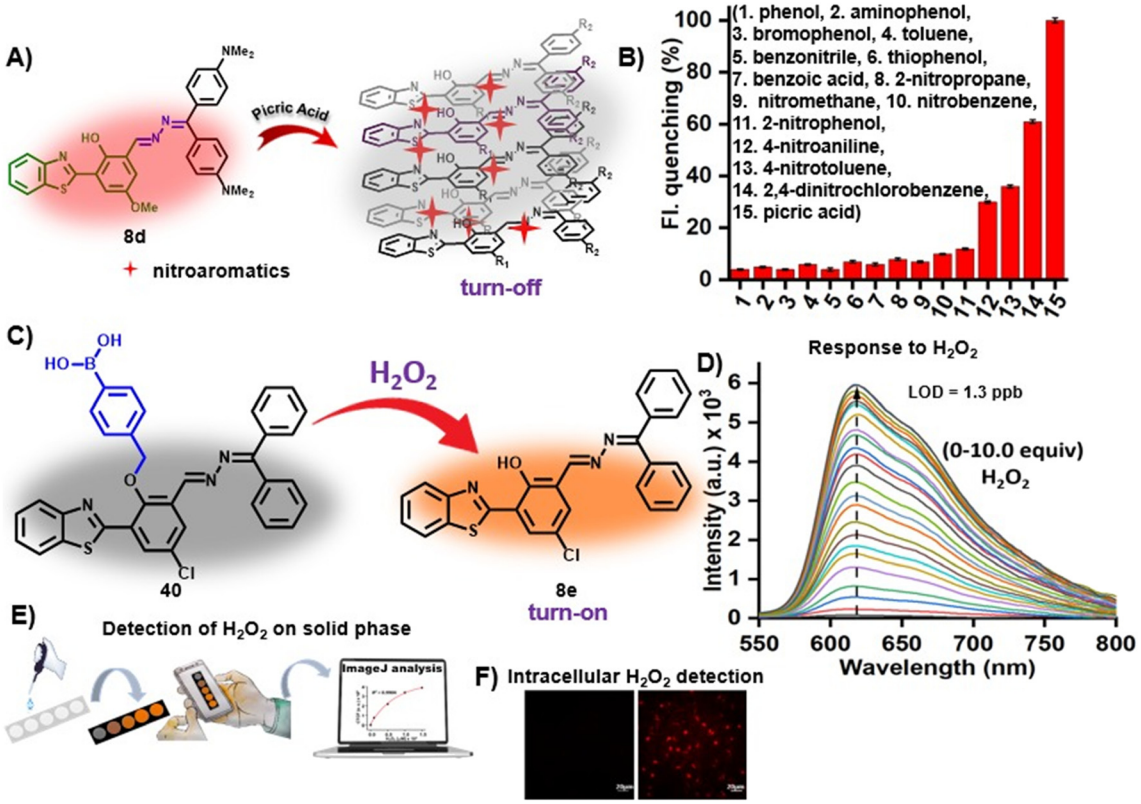

Fig. 6 (A) HBT-based unsymmetrical azine dye (**8d**) as a turn-off chemosensor for the sensitive detection of nitroaromatic compounds showing a turn-off response by disruption in AIE owing to the intercalation of NACs; (B) the fluorimetric responses of **8d** against different analytes depicting the high selectivity of **8d** towards NACs (images A and B are adapted with permission from ref. 37. Copyright 2023, Wiley-VCH); (C) HBT-based chemodosimeter (**40**) for the detection of H_2O_2 ions by cleavage of the benzylboronic acid group; (D) turn-on detection of H_2O_2 ions by **40** with a low detection limit; (E) demonstration of solid-phase detection of H_2O_2 using TLC plates and ImageJ analysis for on-site quantitation of H_2O_2; (F) fluorescence microscopy images of HeLa cells in the presence of **40** and H_2O_2 ions (images C–F are adapted with permission from ref. 90. Copyright 2022, Elsevier).

hazardous substance by US-EPA making its sensitive detection as an important task. Bhattu *et al.* synthesized azine nanoparticles (*E*)-(4-chlorophenyl)-1,1-diamino-2,3-diazabutadiene (**42**) and utilized them for the detection of azinphos-methyl under aqueous conditions [Fig. 7A and Table 3, entry 5].[92] H-bonding interactions between the analyte and guanidine-like unit of the probe, **42**, were responsible for the selective turn-on detection of azinphos-methyl [Fig. 7B]. It showed a limit of detection of 7.4 μM. Its application in real samples like orange juice, water samples, *etc.* showed good recovery and selective fluorescence response. Thiagarajan's group synthesized a new unsymmetrical azine, **43**, and utilized it for the selective and sensitive turn-on detection of the nerve agent mimic diethylchlorophosphate (DCP) by two different mechanisms in different solvent systems [Table 3, entry 6].[93] The photoinduced electron transfer results in a turn-on emission at 495 nm in ACN due to nucleophilic substitution of DCP at the azine nitrogen close to the –OMe group giving rise to a new ICT state [Fig. 7C]. A 1763-fold enhancement in fluorescence was observed with a low detection limit of 9.9 nM. Contrastingly, the protonation at the azine nitrogen in an ACN : H_2O (1 : 4) mixture increased the fluorescence at 422 nm by 1188-fold with a limit of detection of 68 nM [Fig. 7D]. DCP sensing was also demonstrated on TLC strips and polymethylmethacrylate (PMMA) polymer film by coating the probe solution on the solid platforms and then recording the images in the presence and absence of DCP vapors under 365 nm UV light [Fig. 7E]. The absence of DCP vapors showed no fluorescence emission, however, the addition of DCP vapors afforded a green fluorescence indicating the potential of **43** to detect DCP vapors qualitatively from the environmental samples in solid platforms. The same group developed an unsymmetrical D–π–A type azine, **44**, for the detection of DCP by two different channels [Table 3, entry 7].[94] The probe, **44**, forms a new ICT state with DCP in pure THF by phosphorylation at the imine nitrogen close to the donor moiety of **44**. This results in color change to orange with a 203-fold fluorescence enhancement at 513 nm and this moiety acts as a strong withdrawing group. Azine **44** displayed intense fluorescence emission at 570 nm in THF–H_2O fractions which undergoes protonation at the amine nitrogen upon the addition of DCP and causes a blue-shifted emission to 406 nm and fluorescence quenching at 570 nm. The probe also functions as a test-strip based detection assay to detect DCP vapors using Whatman filter paper which

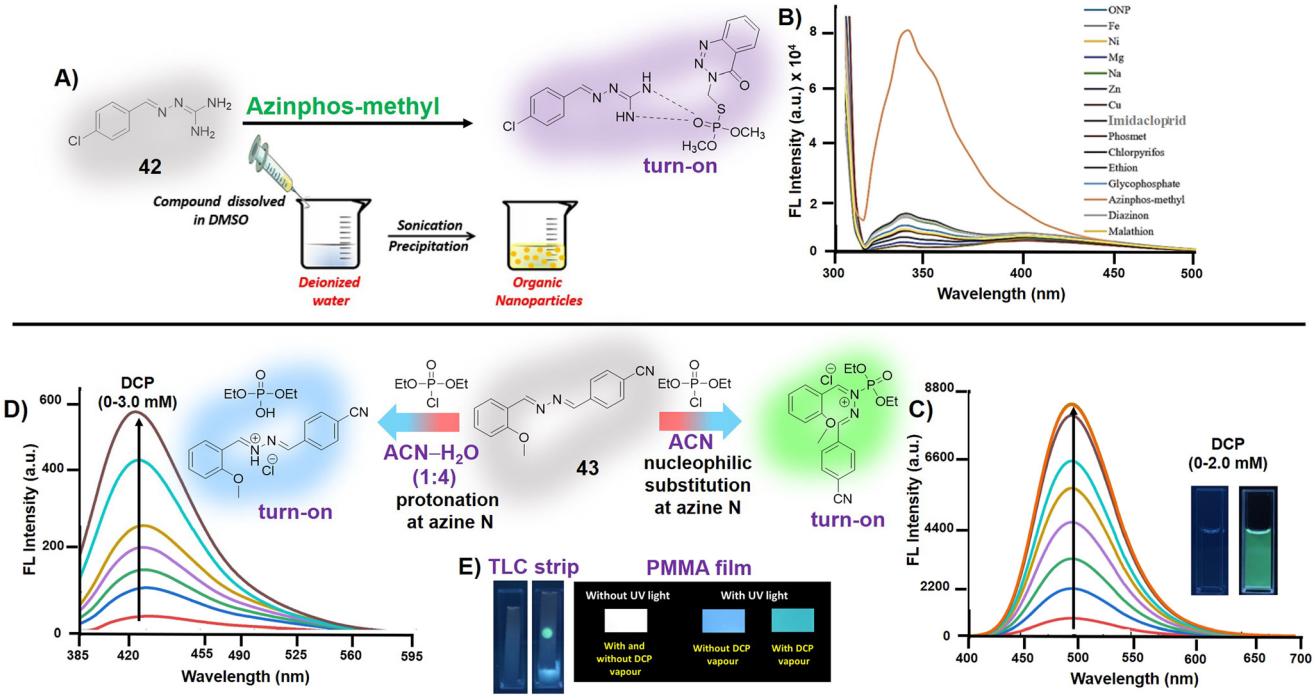

Fig. 7 (A) 1,1-Diaminoazine (**42**) as a chemosensor for organophosphorus pesticide azinphos-methyl; (B) selectivity study of **42** against various OPPs and metal ions (images A and B are adapted with permission from ref. 92. Copyright 2023, Elsevier); salicylaldehyde-based azine (**43**) as a dual-mode chemodosimeter for the detection of nerve agent mimic diethylchlorophosphate (DCP) by (C) turn-on emission at 495 nm in ACN due to nucleophilic substitution of the DCP at the azine nitrogen close to the –OMe group giving rise to a new ICT state and (D) turn-on emission at 422 nm due to protonation at the azine nitrogen in an ACN : H_2O mixture; (E) DCP sensing demonstrated on TLC strips and PMMA polymer film showing green fluorescence emission in the presence of DCP vapors under 365 nm light (images C–E are adapted with permission from ref. 93. Copyright 2021, Elsevier).

displays a visual color change of the test strip from yellow to orange immediately after exposure to DCP vapors.

He *et al.* reported a phosphate-protected salicylaldehyde-based azine (**45**) and utilized it for the detection of alkaline phosphatase in aqueous medium [Fig. 8A and Table 3, entry 8].[95] Additionally, **45** demonstrated strong water solubility and rapid response with a large Stokes shift. The addition of ALP resulted in more than 240-fold turn-on emission intensities [Fig. 8B]. The selectivity study confirmed the sensitive response of **45** towards ALP and no significant change was observed when it is exposed to metal ions, reactive oxygen species, reactive sulfur species (Cys, Hcy, and GSH) and enzymes (esterase, trypsin and lysozyme) [Fig. 8C]. ALP eliminates the phosphate groups of **45** by dephosphorylation affording an intermediate compound that contains one phosphate group and shows very weak fluorescence. The intermediate then undergoes the second dephosphorylation step and releases the unprotected salicylaldehyde-based azine which forms aggregates owing to the intramolecular hydrogen bond and increased hydrophobicity leading to a strong fluorescence signal due to the combined AIE and ESIPT mechanism. Azine-based probe **45** was further explored for differentiating the intracellular ALP activity in different cell lines such as MG-63, WI-38, B6F10, RAW264.7 and HEK293. It was found that MG-63 cells displayed the strongest fluorescence, indicating the highest expression level of ALP in MG-63 cells. WI-38, B16F10 and RAW 264.7 cell lines showed a moderate response, whereas a negligible response was displayed with HEK 293 cells [Fig. 8D]. In addition, MG-63 cells were investigated for the inhibition effect of the ALP inhibitor. The use of 1 mM Na_3VO_4 as an inhibitor showed negligible fluorescence intensity indicating that dephosphorylation of the ALP activity was inhibited by Na_3VO_4 [Fig. 8E].

Tong's group utilized another non-fluorescent azine probe, **46**, protected with a dinitrobenzene sulphonyl group for β-lactamase detection wherein the analyte first reacts with the substrate's lactam (cefazolin sodium) to form a secondary amine, commencing a spontaneous elimination event and yielding a thiol molecule [Fig. 8F and Table 3, entry 9].[96] The thiol reacted with the sulfonate group of **46** to release the salicylaldehyde azine derivative which exhibited AIE–ESIPT properties [Fig. 8G]. β-Lactamase fluorescence measurement afforded a turn-on response at 558 nm with a detection limit of 0.5 mU mL^{-1} [Fig. 8H]. The probe, **46**, was highly selective towards β-lactamase and no other analyte resulted in significant fluorescence emission [Fig. 8I]. Further, **46** was utilized as a portable test paper sensor for the detection of β-lactamase by dipping the filter paper strips coated with **46** into the sample solution containing cefazolin (4.8 mM) and different concentrations of β-lactamase (0–7.0 mU mL^{-1}). A

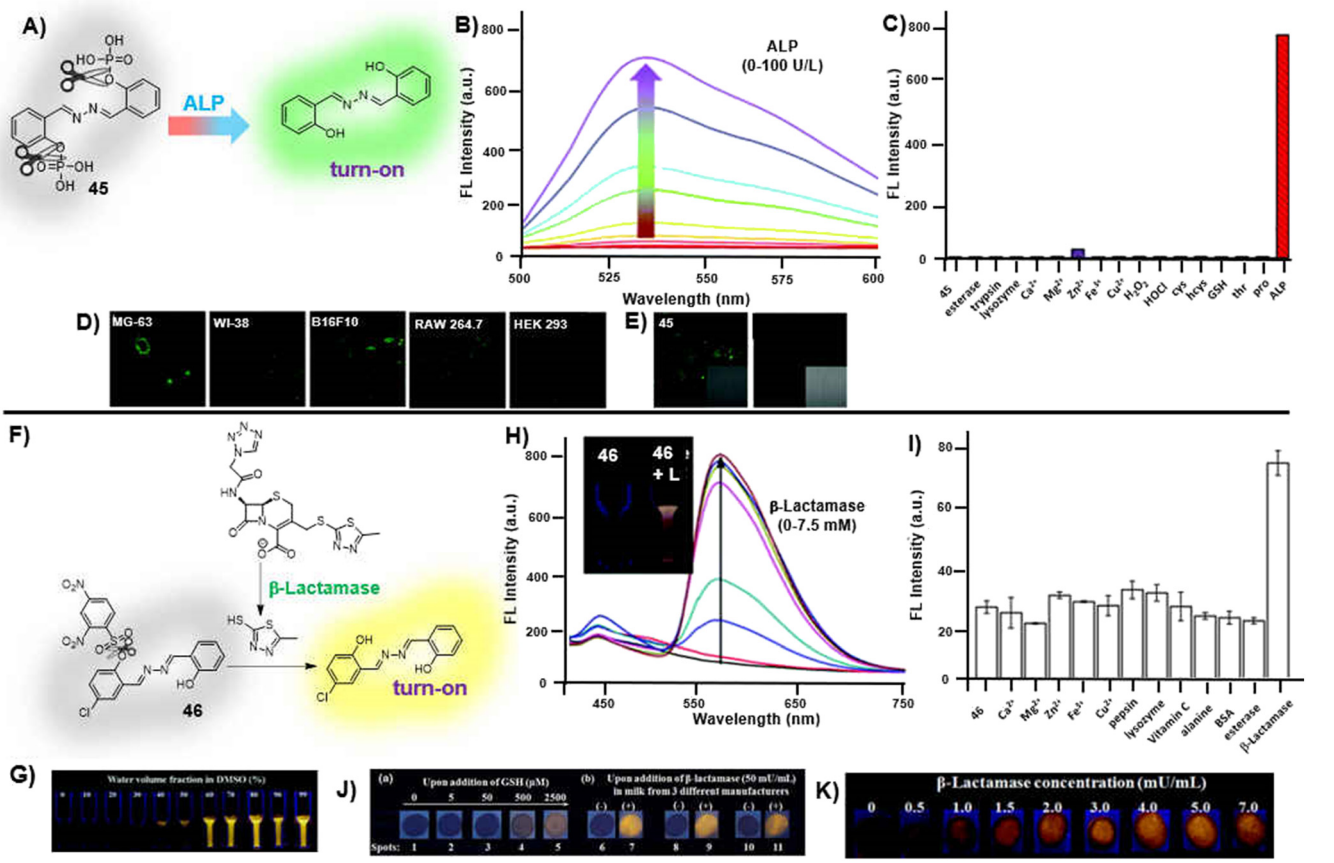

Fig. 8 (A) Salicylaldehyde-based azine (**45**) as a chemodosimeter for alkaline phosphatase by cleavage of the phosphate group; (B) turn-on detection by fluorescence enhancement at 536 nm upon incremental addition of ALP; (C) change in fluorescence intensities towards ALP and various interfering analytes; confocal images of (D) MG-63, WI-38, B16F10, RAW 264.7 and HEK 293 cells after incubation with **45** showing intense fluorescence emission with MG-63 cells indicating the highest ALP expression and (E) MG-63 cells incubated with **45** in the absence and presence of 1 mM Na_3VO_4 wherein the inhibitor results in negligible turn-on response (images A–E are adapted with permission from ref. 95. Copyright 2020, Royal Society of Chemistry); (F) 2,4-dinitrobenzenesulfonyl protected salicylaldehyde-based azine (**46**) as a chemodosimeter for β-lactamase; (G) AIE–ESIPT behavior exhibited by the azine precursor; (H) turn-on detection of β-lactamase by fluorescence enhancement at λ_{max} 558 nm; (I) fluorescence response of **46** towards different metal ions, proteins, enzymes, *etc.* confirming the high selectivity of **46** towards β-lactamase; (J) demonstration of solid-phase detection of β-lactamase on paper-strips; (K) demonstration of solid-phase detection of GSH and β-lactamase in milk samples on paper-strips (images F–K are adapted with permission from ref. 96. Copyright 2018, Royal Society of Chemistry).

good linearity was obtained in the β-lactamase concentration range of 0–2.0 mU mL^{-1} [Fig. 8J]. **46** was also investigated for β-lactamase content in milk samples and the results showed good recoveries, suggesting the potential use for β-lactamase detection in milk samples [Fig. 8K].

Chang *et al.* demonstrated a dual sialic acid-protected salicylaldehyde-derived azine, **47**, for the detection of neuraminidase (NA), a crucial enzyme for the replication of the influenza virus [Fig. 9A and Table 3, entry 10].[97] The initially non-fluorescent probe **47** displayed a turn-on emission at 524 nm with a 30-fold fluorescence enhancement upon the addition of NA having a limit of detection of 0.024 U mL^{-1} due to the cleavage of the sialic acid group [Fig. 9B]. Azine **47** was further explored to detect the influenza virion using hemagglutination (HA) titer for the relative concentration of the virus. H3N2 viruses with different HA titers displayed enhanced fluorescence emission with the increment of H3N2 virions with an LOD of 2^{-1} HAU per 50 μL [Fig. 9C]. The probe **47** in combination with oseltamivir carboxylic acid (OC) was explored to distinguish oseltamivir-resistant mutant type NA (drug-resistant influenza virus strains) from wild types. It was observed that wild-type NA (WT) inhibited the hydrolysis of **47** in the presence of OC, whereas H274Y mutant NA (MT) hydrolyzed **47** both in the presence and absence of OC [Fig. 9D]. The probe, **47**, was employed for NA detection in MDCK cells infected by the influenza virus. MDCK cells infected with H3N2 displayed high fluorescence under confocal imaging whereas the presence of OC showed extremely low background fluorescence [Fig. 9E].

3.4. Azine as dual sensor

AIE-active probes for the simultaneous detection of two or more analytes with distinct emission outputs are rarely cited. Our group envisaged an AIE active NIR-emissive

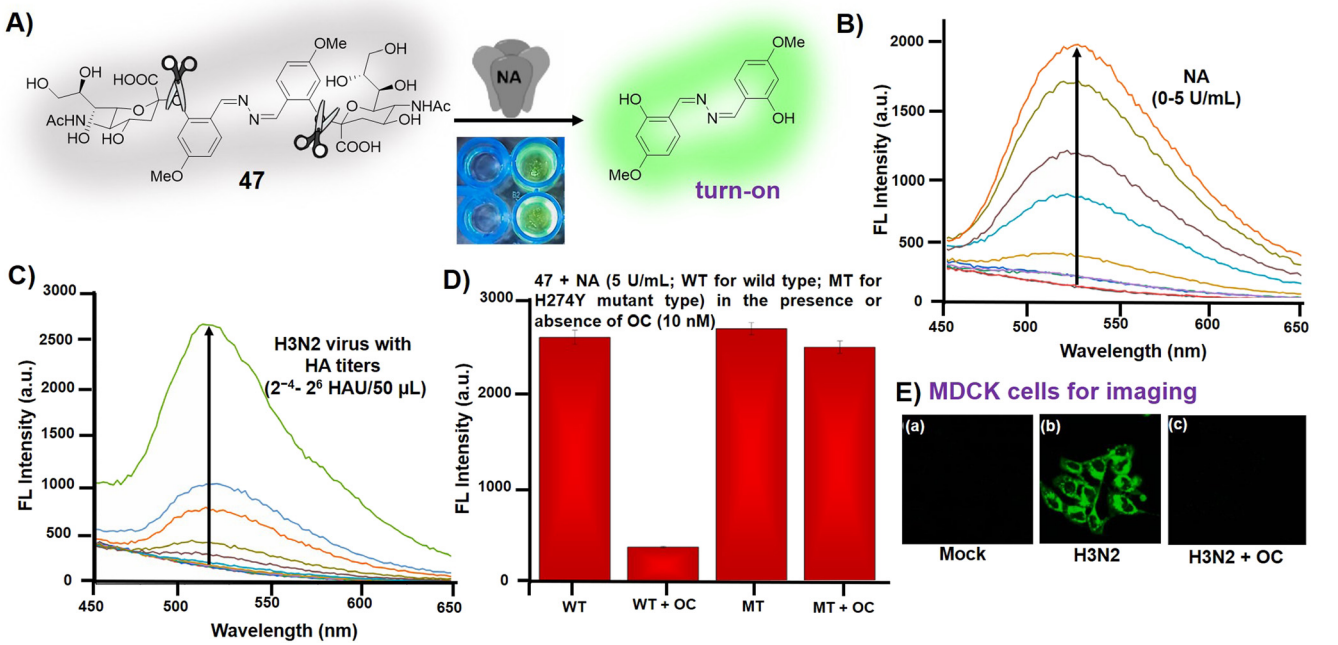

Fig. 9 (A) Salicylaldehyde-based azine, **47**, as a chemodosimeter for the detection of neuraminidase (NA) by cleavage of the sialic acid group; (B) turn-on emission at 524 nm upon addition of NA; (C) turn-on emission at 524 nm upon the addition of different concentrations of H3N2 viruses; (D) fluorescence intensities of **47** after addition of NA showing fluorescence quenching of wild type (WT) in the presence of OC; (E) fluorescence imaging in mock-infected (a), H3N2 infected (b) and OC pretreated infected MDCK cells (c) (adapted with permission from ref. 97. Copyright 2022, Elsevier).

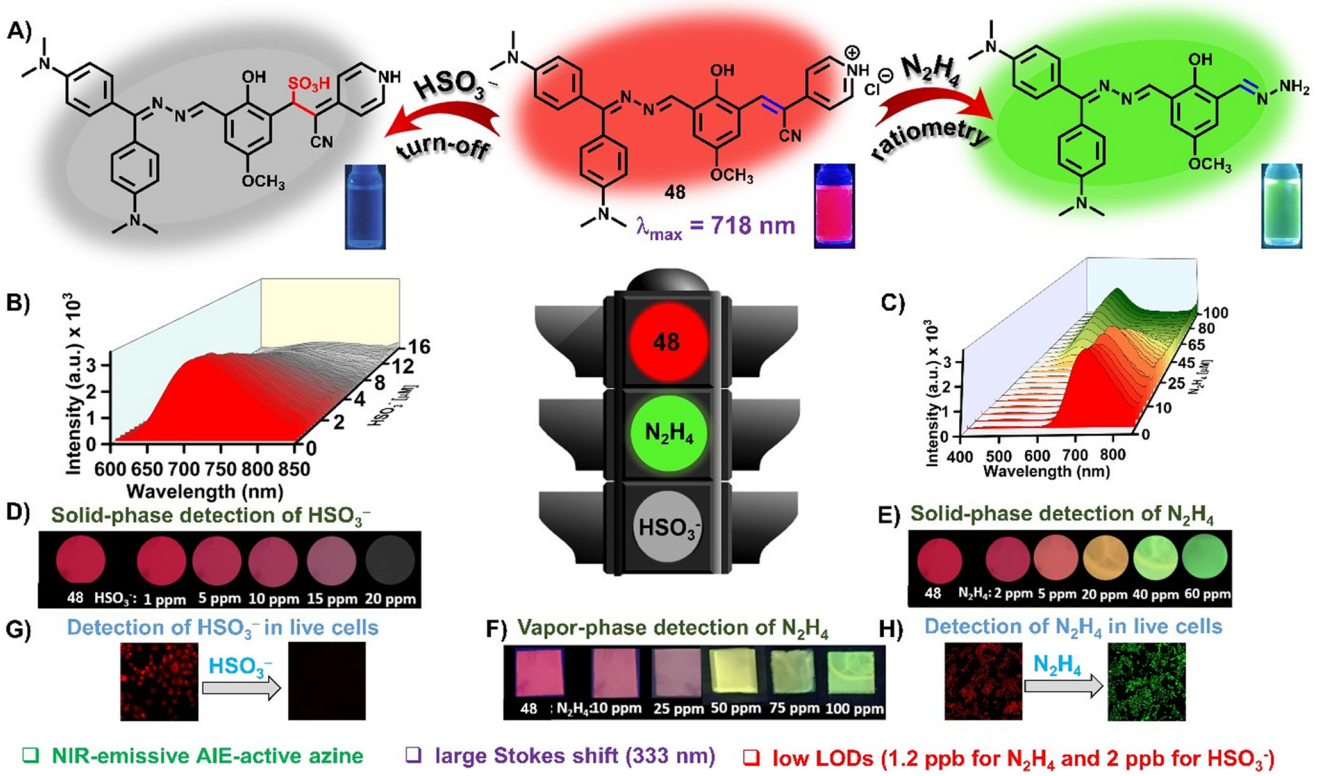

Fig. 10 (A) NIR-emissive cationic azine (**48**) as a dual-chemodosimeter for N_2H_4 and HSO_3^- ions; (B) turn-off detection of HSO_3^- ions by addition across the double bond of the azine; (C) ratiometric response in the presence of N_2H_4 by cleavage of the cyano pyridyl group; demonstration of solid-phase detection of (D) N_2H_4 and (E) HSO_3^- ions; (F) demonstration of vapor-phase detection of N_2H_4; (E) fluorescence microscopy images of A549 cells in the presence of **48** and (G) N_2H_4 and (H) HSO_3^- ions (adapted with permission from ref. 30. Copyright 2023, Elsevier).

unsymmetrical azine, benzophenone-azine-phenyl-cyanovinyl-pyridinium chloride (**48**), as a dual-mode-dual-chemodosimeter for the selective and sensitive detection of toxic analytes, N_2H_4 and HSO_3^- [Fig. 10A].[30] The D–π–A azine was designed to emit in the NIR region by keeping the electron-donating 4,4′-(hydrazineylidenemethylene)bis(*N*,*N*-dimethylaniline) and the electron-withdrawing cyano-pyridinium ethylene moiety at either ends of the azine linkage. The azine, **48**, was synthesized by adopting one-pot tandem mechanochemistry. It displayed emission at 718 nm upon excitation at 385 nm with a large Stokes shift of 333 nm in 1% DMSO/H_2O. The presence of two strong electron-withdrawing groups *viz.* –CN and $-Py^+$ in the probe ensured a quick turn-off response against HSO_3^- by addition across the double bond and a ratiometric response at 525 nm against N_2H_4 by cleaving the cyano pyridyl group [Fig. 10B and C]. The excellent selectivity of **48** in the presence of other competing amines, cations, and anions resulted in a limit of detection (LOD) of 4×10^{-8} M (1.2 ppb) and 2.5×10^{-8} M (2 ppb) for N_2H_4 and HSO_3^-, respectively. The practical utility of the probe has been established for solid-phase and vapor-phase detection of the analytes on silica-coated TLC plates, followed by ImageJ analysis for on-site quantitation, and the real sample analysis was validated by spiking the analytes in various water, soil, and food samples [Fig. 10D–F]. The probe, **48**, has also been utilized to detect intracellular N_2H_4 and HSO_3^- in living cells [Fig. 10G and H]. The sustainable tandem mechanochemical synthesis, NIR emission with large Stokes shift, ratiometric response, high selectivity and sensitivity, low response time, LOD in the ppb range, on-site solid-phase and vapor-phase detection, and potential in detection of the analytes in live cells are some of the merits of the sensing system.

3.5. Azines in multi-targeted sensing

Chemosensors capable of sensitively detecting multiple analytes with different fluorescence outputs are handy as they offer advantage of cost-efficient analysis when compared with single analyte-specific sensors.[98] Azines have been occasionally used for multi-analyte detection. In this direction, Yadav *et al.* demonstrated an azine (**49**) for the multi-targeted sensing of metal ions, viscosity and pH sensing [Fig. 11].[99] The azine-based probe, **49**, displayed a distinctive color change to brown, dark yellow and greenish yellow and acts as a selective colorimetric sensor for Co^{2+}, Cu^{2+} and Zn^{2+} ions, respectively, in DMF : water (9 : 1 v/v, HEPES 10 mM). However, the turn-on response in

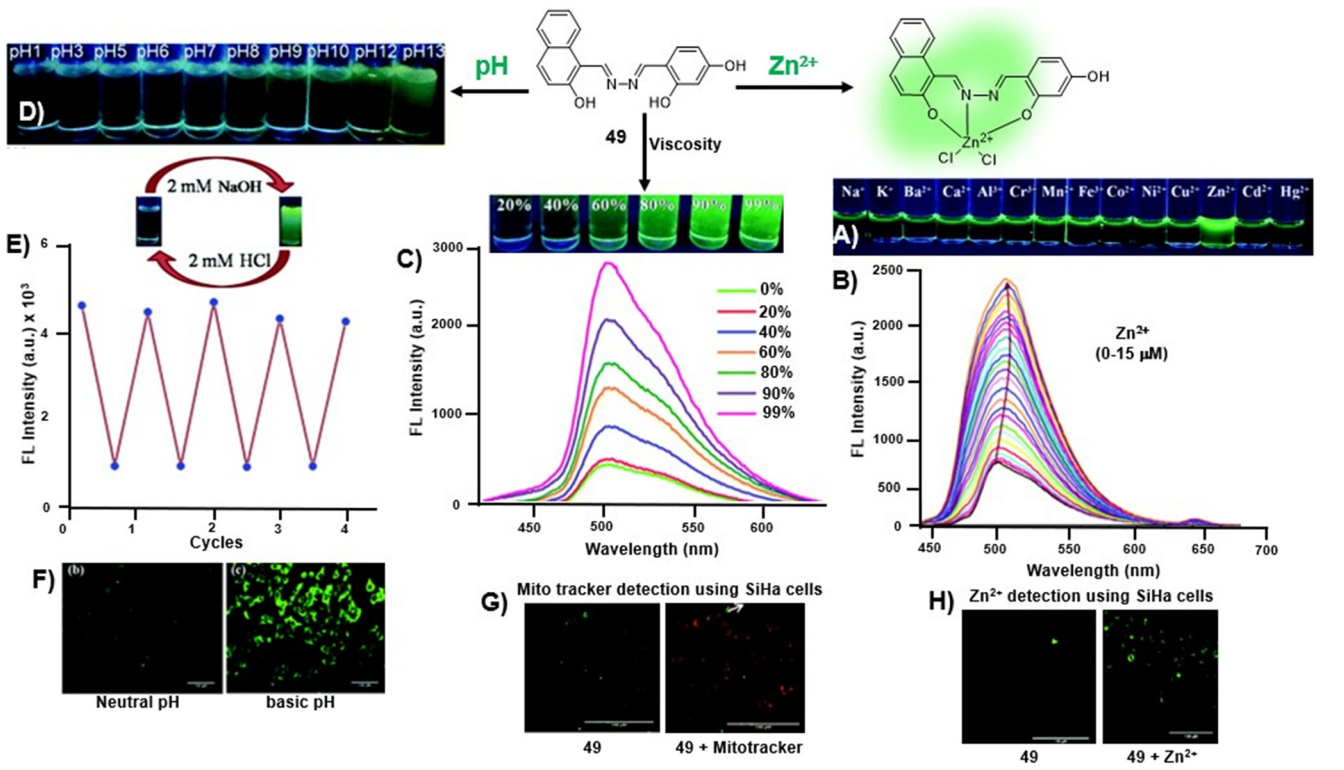

Fig. 11 (A) The fluorometric responses of **49** against various metal ions captured under 365 nm UV-light showing selective turn-on response towards Zn^{2+} ions; (B) turn-on fluorescence response of **49** at 500 nm upon incremental addition of Zn^{2+} ions; (C) the change in the fluorescence emission of **49** at various DMF : glycerol mixtures and its corresponding images captured under 365 nm UV-light showing stronger emission at higher glycerol fractions; (D) the fluorimetric changes displayed by **49** as a function of pH captured under 365 nm UV-light; (E) the reversible behavior of **49** demonstrated against NaOH and HCl showing high reusability up to 4 cycles; fluorescence microscopy images of SiHa cells studied against (F) pH variation, (G) Mito tracker activity and (H) Zn^{2+} detection (adapted with permission from ref. 99. Copyright 2022, Royal Society of Chemistry).

fluorimetric studies was found to be highly specific towards Zn^{2+} ions [Fig. 11A]. The probe exhibits a fluorescence turn-on response towards Zn^{2+} ions with an increase in emission intensities at 500 nm and displayed a lower LOD of 37 nM [Fig. 11B]. The azine **49** demonstrates remarkable viscochromism in DMF : glycerol medium wherein with increasing viscosity a noteworthy 6-fold increase in the fluorescence intensity was observed [Fig. 11C]. At lower glycerol fractions, the skeletal framework of **49** rotates freely which relaxes the excited state through a non-radiative decay process. However, at higher glycerol fractions, intramolecular rotation around N–N bonds is restricted leading to strong green fluorescence. Similarly, **49** displayed a turn-on response against increasing pH and acts as a turn-on sensor for basic pH indicators [Fig. 11D]. The negligible fluorescence of **49** in the pH range of 2 to 9 enhanced rapidly in basic pH and a 5-fold enhancement in fluorescence intensity was observed at pH 13 owing to the deprotonation of phenolic hydroxyl protons. The reversibility of **49** towards acidic and basic media by subsequent addition of NaOH and HCl showed that the probe could detect the pH changes significantly for four cycles without much change in its responses [Fig. 11E]. Further, live cell imaging on SiHa cells has been demonstrated for the intra-cellular detection of Zn^{2+}, basic pH and in mitotracking and monitoring cytoplasmic viscosity changes in SiHa cells [Fig. 11F–H]. It efficiently identified the apoptosis process by exhibiting an increase in fluorescence intensity, transitioning from cancerous SiHa cells to apoptotic cells.

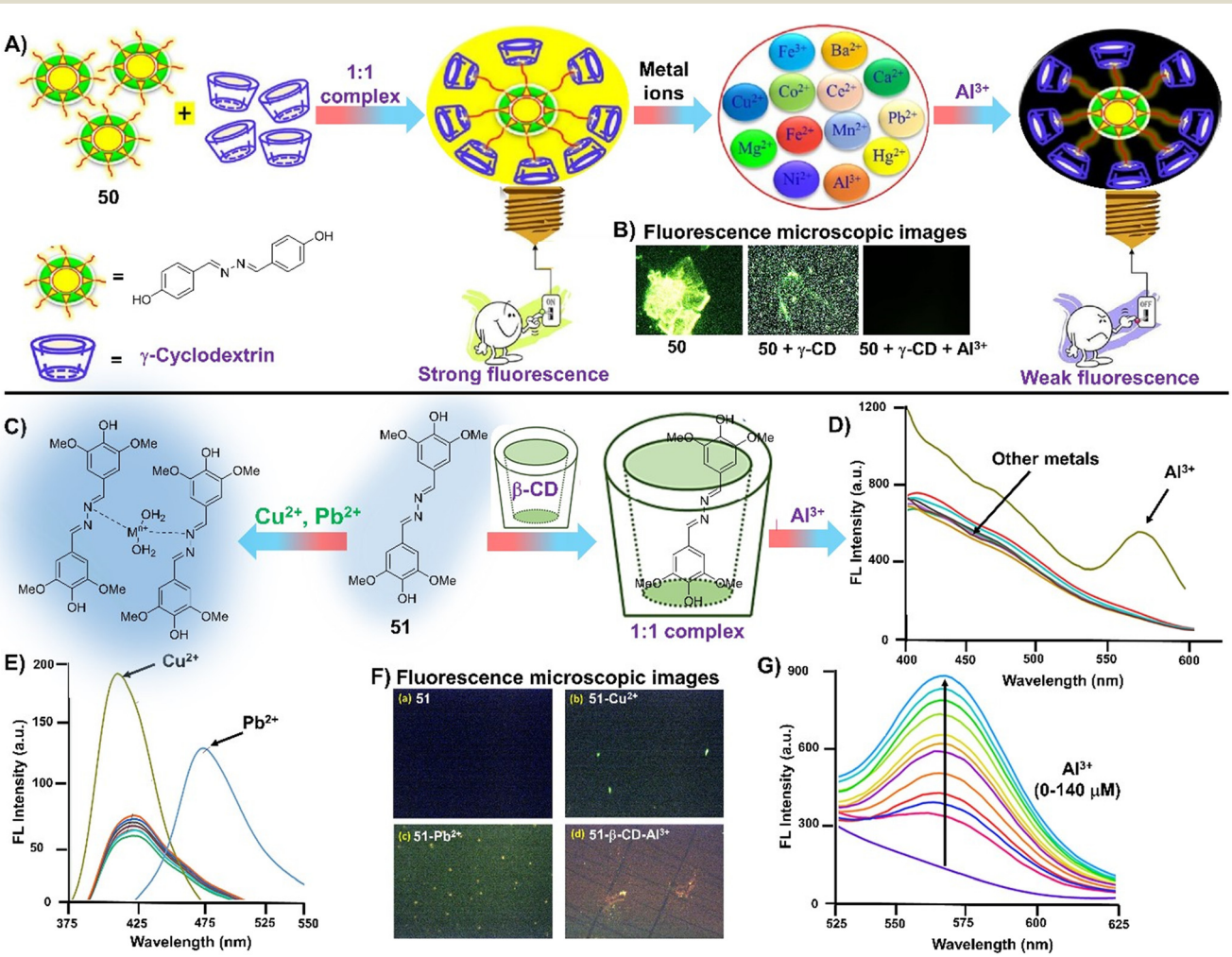

Fig. 12 (A) Salicylaldehyde azine with terminal phenolic –OH (**50**) forming a strongly fluorescent 1 : 1 inclusion complexation with γ-CD which acts as a turn-off chemosensor for supramolecular sensing of Al^{3+} ions; (B) fluorescence microscopy images of **50** in the presence of γ-CD and Al^{3+} ions displaying a turn-off sensing response (images A and B are adapted with permission from ref. 103. Copyright 2023, Elsevier); (C) syringaldehyde-based azine (**51**) as a chemosensor for Cu^{2+} and Pb^{2+} ions by CHEF and LMCT pathways, respectively; (D) the fluorescence enhancement of **51** with Cu^{2+} at 413 nm and Pb^{2+} ions at 473 nm; (E) the **51** : β-CD inclusion complex displaying high selectivity towards Al^{3+} without any interference from Cu^{2+} and Pb^{2+}; (F) **51** : β-CD complex displays a turn-on response against Al^{3+} addition with an increase in fluorescence intensity at 573 nm; (G) confocal fluorescence imaging indicating fluorescence enhancement with Cu^{2+} and Pb^{2+} in the green region and the red emission obtained after the **51** : β-CD complex reacts with Al^{3+} ions (images C–G are adapted with permission from ref. 104. Copyright 2023, Elsevier).

4. Azines in supramolecular sensing

A supramolecular sensor generally helps in the detection of a particular analyte by the formation of a conjugate with a supramolecular host *via* host–guest interactions mediated by H-bonding, π–π interaction, *etc.* which upon the addition of the analyte displaces the probe from the complex and results in a fluorescence change. Similarly, amphiphilic AIE polymers can self-assemble in a selective medium resulting in various interesting nanostructures with turn-on fluorescence. The analyte can trigger a disassembly to generate a measurable optical change. The dynamic non-covalent interactions and adaptive nature of the supramolecular assemblies towards different sensing environments result in a selective and sensitive detection tool for a particular target analyte.[100,101]

4.1. Host–guest based sensors

Macrocyclic structures are frequently involved in supramolecular host–guest interactions, which have been established as recognition units in the sensing assembly.[102] The non-covalent trapping of analytes as guest molecules in the host cavity serves as the basis for the molecular recognition process for the majority of macrocyclic hosts. These macrocycles are chemically stable, simple to functionalize, and are excellent receptors for a variety of analytes as guest molecules. The cyclization of various aryl motifs through short linkers can produce macrocycles with various functionalities, often consisting of a hydrophobic inner half and a hydrophilic outer part.

Ganesan *et al.* synthesized a symmetrical azine 4,4′-((1*E*,1′*E*)-hydrazine-1,2-diylidenebis(methanylylidene)) diphenol (**50**) from 4-hydroxybenzaldehyde and utilized it for a 1 : 1 inclusion complex formation with γ-cyclodextrin [Fig. 12A].[103] The azine, **50**, displayed poor water solubility, and thus resulted in weak fluorescence emission. The inclusion complexation of γ-CD/**50** in an aqueous medium increased the water solubility and favored the metal ion sensing phenomenon. The fluorescent assembly was able to detect

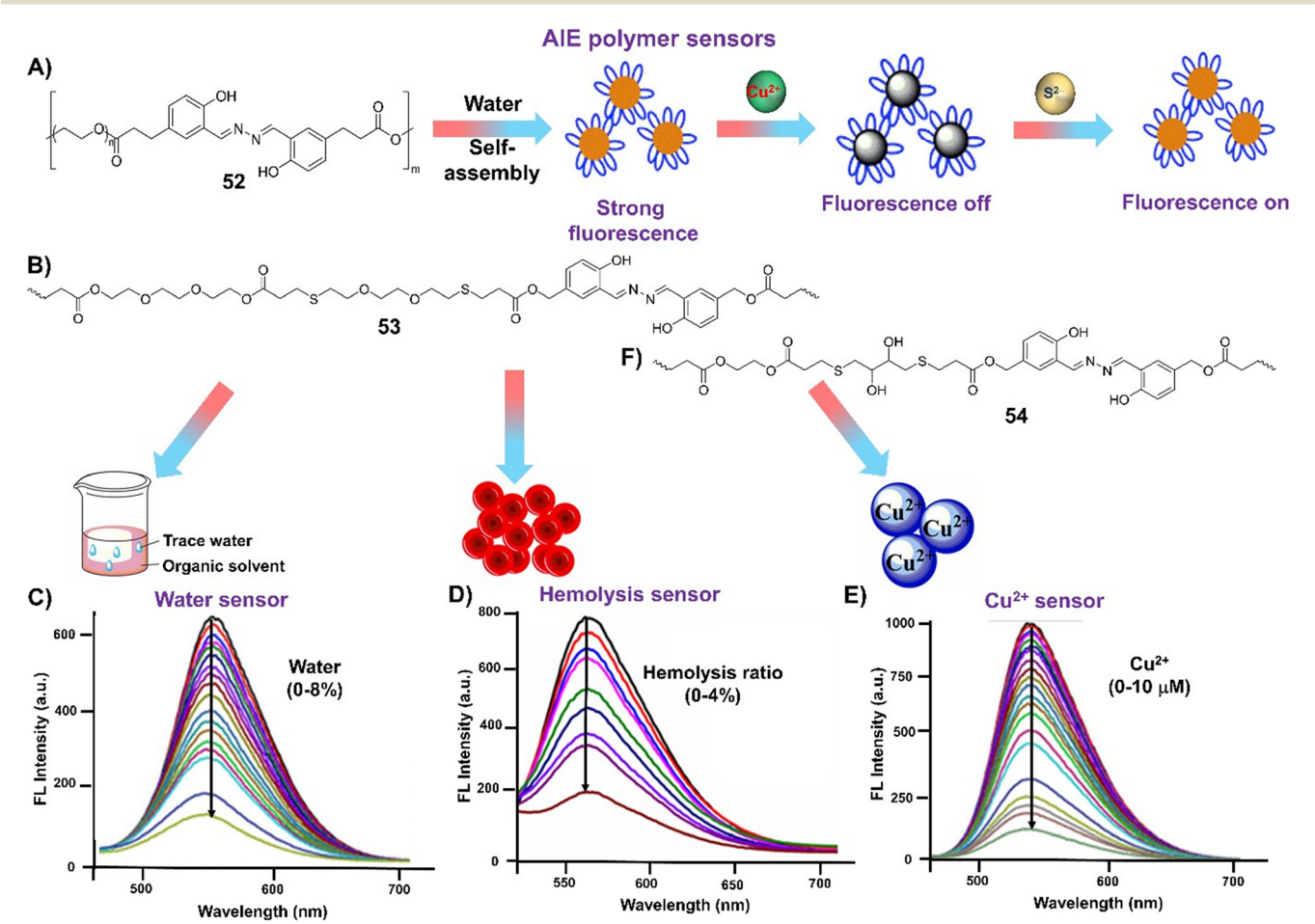

Fig. 13 (A) Utilization of salicylaldehyde-based azine for preparation of AIE-polymer **52** and its response towards Cu^{2+} and S^{2-} ions (image A is adapted with permission from ref. 107. Copyright 2020, Elsevier); (B) and (F) AIE-active polymers **53** and **54** with salicylaldehyde backbones in the main chain *via* thiol–ene click copolymerization, respectively; (C) fluorescence response of **53** as a function of water content (0 to 8%) showing a decrease in intensity upon addition of water fractions to the amide solvents; (D) decrease in the fluorescence intensity of the supernatant from RBC solutions as a function of hemolysis ratio (0 to 4%); (E) turn-off response displayed by **53** upon addition of Cu^{2+} ions (images C–E are adapted with permission from ref. 108. Copyright 2021, American Chemical Society).

Al^{3+} selectively and sensitively in the presence of different analytes. The formation of a stable 1 : 1 complex with Al^{3+} which predominantly uses their –OH and –N atoms afforded an LOD of 1.67 nM. The probe, **50**, was further employed for fluorescence microscopy imaging which displayed a fluorescence quenching phenomenon upon the addition of Al^{3+} ions to the γ-CD–**50** complex [Fig. 12B].

Narayanan *et al.* demonstrated a symmetrical azine (**51**) based on syringaldehyde for the dual detection of metal ions (Cu^{2+} and Pb^{2+}) in different mechanistic pathways [Fig. 12C].[104] The addition of Cu^{2+} to the azine solution resulted in an enhancement in the emission intensity at 413 nm *via* the chelation enhanced fluorescence mechanism (CHEF), whereas, in the case of Pb^{2+} ions, an enhancement in emission intensities with a red-shift to 473 nm was observed due to ligand to metal charge transfer (LMCT) [Fig. 12D]. Interestingly, the inclusion complex of **51** with β-cyclodextrin increases the water solubility and sensing probability and detects Al^{3+} without any interference from Cu^{2+} and Pb^{2+}. The high selectivity towards Al^{3+} may be attributed to the interaction of the hydroxy group of β-CD with the metal ion [Fig. 12E]. The **51** : β-CD complex displays a turn-off response which gets drastically changed when Al^{3+} was added to the supramolecular conjugate and an increase in fluorescence intensity at 573 nm was obtained with a detection limit of 3.2 μM [Fig. 12F]. The fluorescence imaging studies were conducted using confocal microscopy which indicated that the presence of Cu^{2+} and Pb^{2+} enhances the green fluorescence and in the case of **51** : β-CD + Al^{3+} a red emission is obtained [Fig. 12G].

4.2. Azine-polymer sensors

In recent years, the utilization of AIE polymers as sensors for different analytes has received considerable interest.[105] AIE polymers are associated with numerous advantages such as tunable solubility, high thermal stability, good processability, biocompatibility, structural and functional diversity in comparison to AIE-active small molecules.[106] Polymers with AIEgens in the mainchain or sidechain are quite vital in films and gel materials. As of now, numerous AIE-active azine-based polymers have been demonstrated.

Huang *et al.* demonstrated a salicylaldehyde-based azine polymer with PEG arms (**52**) [Fig. 13A].[107] Due to the hydrophilic PEG segments and hydrophobic salicylaldehyde moieties in the core, the polymer self-assembles into stable micelles in water at ambient temperature and fluoresces orange. Polymer micelles, produced at ambient temperature, can be used as a turn-off fluorescent probe to selectively detect Cu^{2+} in aqueous environments with a low detection limit of 53 nM. The **52**–Cu^{2+} complex can be employed as a

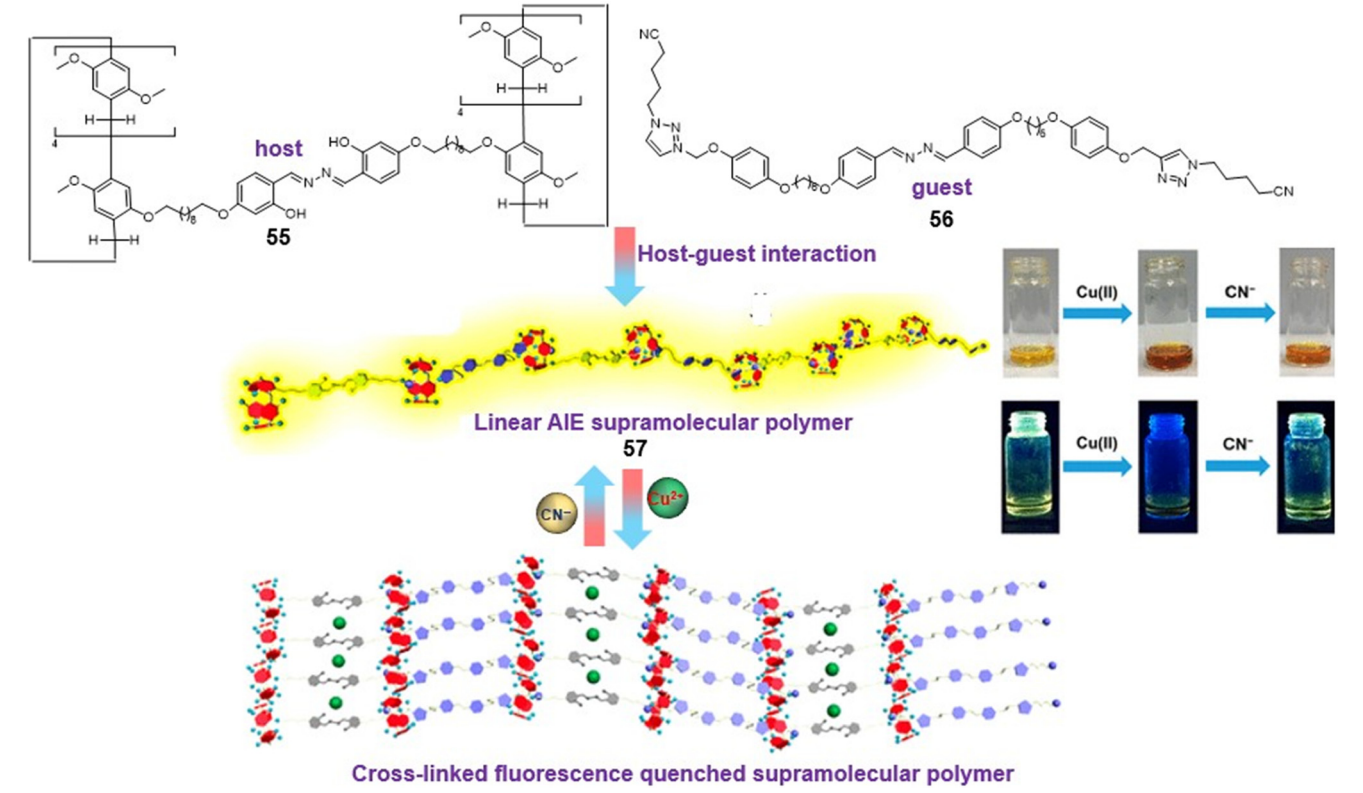

Fig. 14 Salicylaldehyde azine-containing pillar[5]arene dimer as a supramolecular assembly for detection of Cu^{2+} and CN^- ions (adapted with permission from ref. 110. Copyright 2019, American Chemical Society).

turn-on fluorescent probe for the selective detection of S^{2-} displaying an LOD of 0.24 μM.

Lu and co-workers used thiol–ene click copolymerization of the SA derivative diacrylate monomer, poly(ethylene glycol) diacrylate and 3,6-dioxa-1,8-octanedithiol for the preparation of a multi-functional polymer (**53**) [Fig. 13B].[108] **53** unexpectedly exhibited intense emission in amide solvents, which gets significantly reduced by the addition of a small amount of water, serving as a water trace indicator in amide solvents [Fig. 13C]. Secondly, the presence of PEG segments facilitated its dispersion in water and the ROS-responsive thioether groups made it a promising scavenger for reactive oxygen species (ROS) [Fig. 13D]. Additionally, the azine moieties served as a fluorescent indicator for hemolysis determination and selective Cu^{2+} detection owing to the binding capacity of the azine [Fig. 13E]. The same group further demonstrated another amphiphilic AIE-active polymer with dithiothreitol, poly(ethylene glycol) diacrylate, and a salicylaldehyde-based azine (**54**) with increased water solubility [Fig. 13F].[109] PEG segments and DTT units formed stable micelles to help the polymer disseminate in water and preferentially complex with Cu^{2+}, making it a fluorescent sensor in aqueous media.

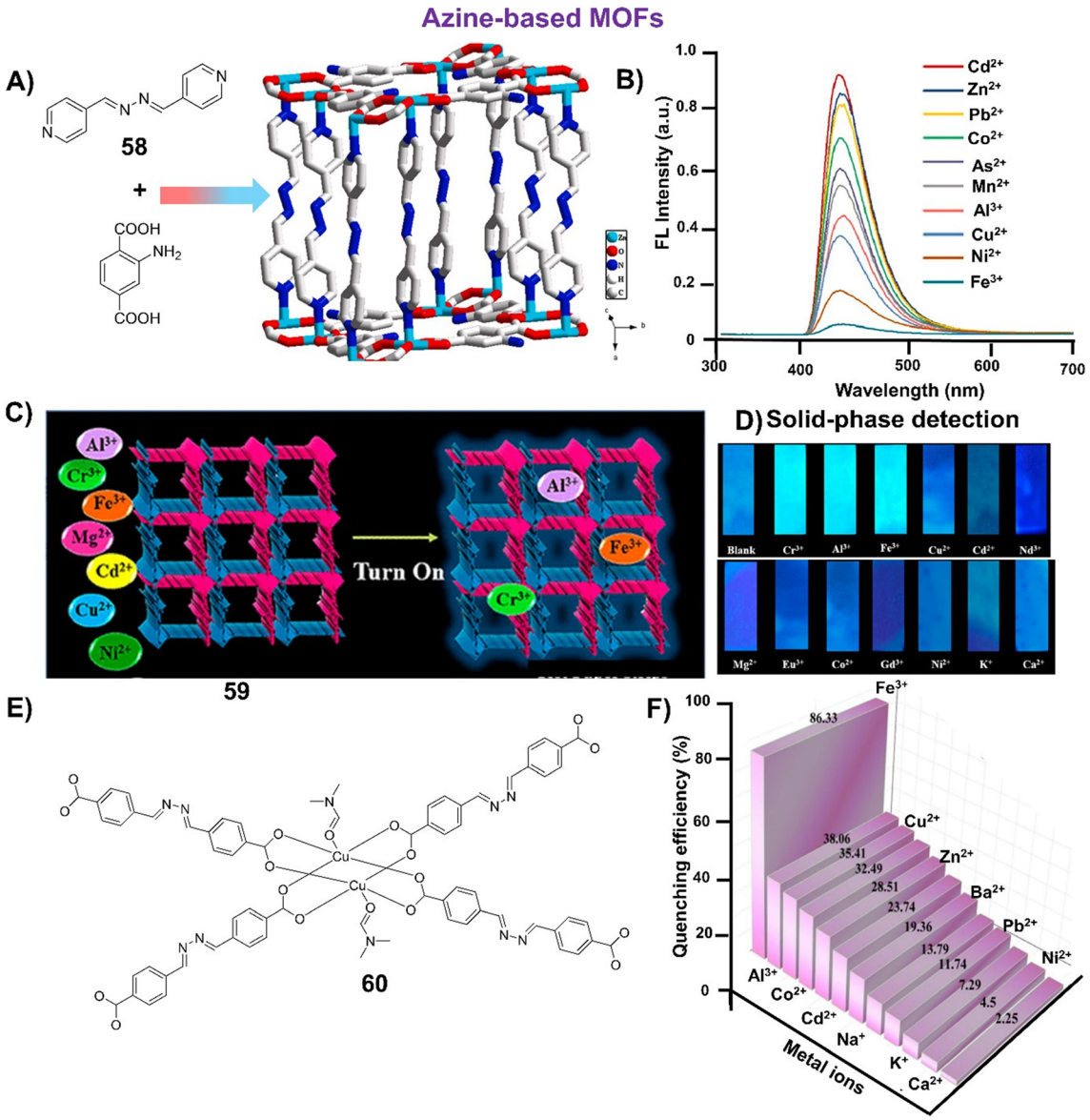

Fig. 15 (A) Demonstration of a pyridyl-azine (**58**) for the formation of the cuboidal block Zn-based MOF showing Zn units linked by eight units of **58** and eight units of the amino-1,4-benzenedicarboxylic acid; (B) emission spectra of the Zn-based MOF against various metal ions showing the highest response towards Fe^{3+} (images A and B are adapted with permission from ref. 113. Copyright 2019, Elsevier); (C) pictorial description of a 3D porous Zn-based luminescent MOF (**59**); (D) test papers strips coated with **59** showing selective turn-on response towards metal ions such as Cr^{3+}, Al^{3+} and Fe^{3+} under 365 nm UV-light (images C and D are adapted with permission from ref. 114. Copyright 2022, American Chemical Society); (E) core structure of the luminescent Cu^{2+}-based MOF (**60**) with Lewis basic Schiff base sites; (F) % quenching depicted by the Cu-based MOF **60** against different metal ions (image F is adapted with permission from ref. 115. Copyright 2023, Springer).

Wang *et al.* reported a linear AIE supramolecular polymer (**57**) from a salicylaldehyde azine-containing pillar[5]arene dimer (**55**) and an azine-based homoditopic guest (**56**) and utilized it as a turn-off Cu^{2+} sensor [Fig. 14].[110] The polymer, **57**, was strongly fluorescent at high concentration and the addition of Cu^{2+} ions results in quenching of the fluorescence as the linear supramolecular polymer changes into a cross-linked supramolecular polymer. The fluorescence of the sensor was re-established upon the addition of CN^- ions. The cross-linkable AIE supramolecular polymer fabricated by the salicylaldehyde azine-containing pillar[5] arene dimer serves as a promising candidate for advanced materials such as metallogels, sensors, and adaptive coatings.

4.3. Azine-MOF as sensors

Metal–organic frameworks (MOFs) have been of great research interest for the detection of metal ions, anions, *etc.*[111] They are formed by the coordination bonding of metal centers and organic linkers and usually display a high surface area, porosity, rich structural diversity, availability of in-pore functionality and scope for outer-surface modification. In particular, luminescent MOFs exhibit easily induced luminescence, low cost, high selectivity and sensitivity, diverse component scope and various detecting mechanisms.[112] MOF fluorescent sensors typically respond by fluorescence enhancement or quenching depending upon the incorporation of guest molecules and ions into their pores.

Farahani *et al.* utilized a pyridyl-based azine (**58**) to prepare a Zn-based metal–organic framework that could selectively detect Fe^{3+} ions in DMF [Fig. 15A].[113] The photoinduced electron transfer between the Fe^{3+} ions and the ligand with the amino-functionalized structure in this MOF is responsible for the effective fluorescence quenching action. In addition, the azine –N donors also contribute their lone-pair electrons to the Fe^{3+} ions resulting in a notable improvement in the detection capability. With a response time of less than one minute and a detection limit of 0.7 μM, the detection of Fe^{3+} was highly selective, and there were no interferences from As^{3+}, Cd^{2+}, Zn^{2+}, Co^{2+}, Ni^{2+}, Cu^{2+}, Pb^{2+}, Mn^{2+}, and Al^{3+} [Fig. 15B].

Mukherjee *et al.* developed another substituted pyridyl-based azine probe and used it in the preparation of a highly scalable 3D porous Zn-based MOF **59** by following a mixed ligand synthesis approach [Fig. 15C].[114] The aromatic π-conjugated organic linker and N-rich spacer incorporating azine functionality as binding sites for metal ions immobilized within the pore spaces have rendered this MOF an excellent turn-on sensor. A turn-on phenomenon of this nature is uncommon, and a thorough examination indicated an enhancement mechanism attributed to absorbance, known as the absorbance-caused enhancement (ACE) mechanism. It exhibits exceptional sensitivity, selectivity and

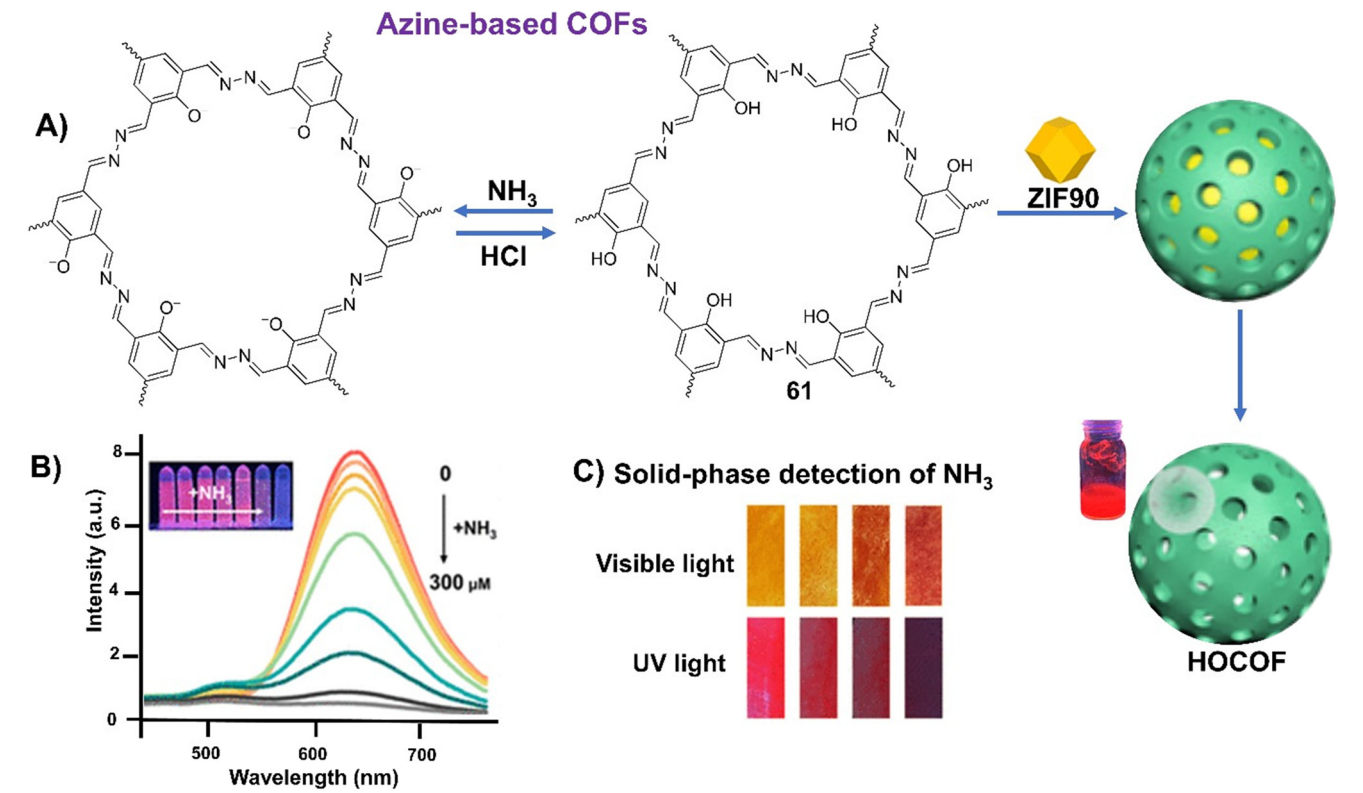

Fig. 16 (A) Azine-based emissive COF (**61**) showing turn off/on reversible response against NH_3/HCl. Further utilization of **61** for the hollow COF by the sacrificial template strategy; (B) turn-off fluorescence response displayed by HOCOF with different concentrations of NH_3; (C) paper-based HOCOF sensor upon exposure to NH_3 for different times (adapted with permission from ref. 118. Copyright 2023, American Chemical Society).

recyclability for Al^{3+}, Cr^{3+} and Fe^{3+} ions. The azine MOF, **59**, was further utilized as a simpler, convenient and portable solid-phase detection tool for the sensing of metal ions by turn-on response [Fig. 15D]. The visualization of the MOF **59** loaded silica gel test strips under 365 nm UV-light displayed an enhancement in the fluorescence emission against Cr^{3+}, Al^{3+} and Fe^{3+}, whereas no change was noted for the other metal ions. In a similar approach, Kaur *et al.* synthesized a Cu^{2+}-based MOF **60** through the solvothermal method and demonstrated it as a highly selective sensor towards Fe^{3+} with a low LOD of 47 ppb [Fig. 15E].[115] The sensing ability of **60** towards Fe^{3+} was evaluated against different metal ions and it was noted that no significant quenching was displayed by Ca^{2+}, Ni^{2+}, K^{+}, Pb^{2+} and Na^{+} [Fig. 15F]. Ba^{2+}, Cd^{2+}, Zn^{2+}, Co^{2+}, Cu^{2+} and Al^{3+} showed a reasonable quenching effect, but the % quenching of 86% shown by Fe^{3+} ions was the best among the selected metal ions.

4.4. Azine-COF as sensors

Covalent organic frameworks (COFs) stand out as crucial and dynamic constituents within the category of porous organic materials.[116] They are assembled through reticular chemistry, where building blocks are linked by covalent bonds. Their intriguing characteristics, including the substantial surface area, structural adaptability, ease of surface modification, and strong chemical stability, contribute to their significance. Numerous materials belonging to this class have been created and applied across various disciplines.[117]

Xia *et al.* synthesized a salicylaldehyde azine-based 2D-COF (**61**) through the condensation of two non-AIE monomers, 2-hydroxy-1,3,5-triformylbenzene and hydrazine [Fig. 16A].[118] The dispersibility and accessibility of the COF were improved by growing the COF *in situ* on ZIF-90 followed by digestion under mild acidic conditions to form a hollow COF (HOCOF) with a well-designed AIE structure, excellent dispersibility, small size, and low density. The strong red emission of the HOCOF at 635 nm was completely quenched by ammonia (NH_3) owing to the break in the hydrogen bonding and unlocking of the rotors of azine segments thereby disabling the AIE modules [Fig. 16B]. The HOCOF displayed a low limit of detection of 157 nM and a broad response range of 0.1–300 μM for the detection of NH_3. Further paper-based sensors were

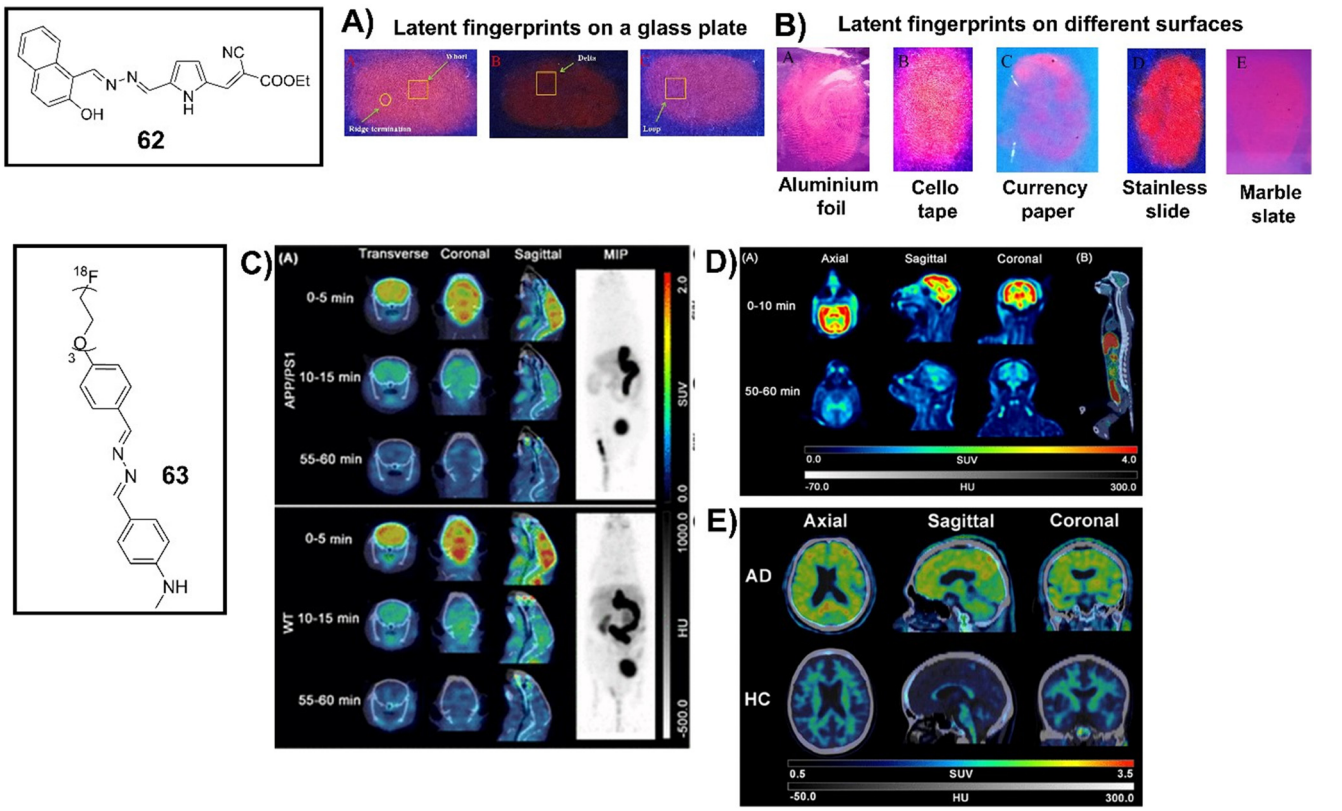

Fig. 17 (A) and (B) Latent fingerprints of different individuals developed on glass TLC plates and various other surfaces such as aluminium foil, cello tape, currency paper, stainless slide, and marble slate showing the variable scope of latent fingerprinting regardless of the surface under investigation (images A and B are adapted with permission from ref. 120. Copyright 2023, Elsevier); (C) fusion images (transverse, coronal, and sagittal) of dynamic micro-PET/CT study of **63** in APP/PS1 mice and WT mice at different time intervals with the maximum intensity projection (MIP) image at 55–60 min after intravenous administration of **63**; (D) fusion images (axial, sagittal, and coronal) of PET/CT study of **63** in the rhesus monkey's head at 0–10 min and 50–60 min post-injection along with the whole-body image at 60–70 min post-injection; (E) PET/CT images after injection in an AD patient and a HC subject showing accumulation of **63** in the cortex while the retention of **63** was mainly in the white matter in the HC subject (images C–E are adapted with permission from ref. 122. Copyright 2023, American Chemical Society).

demonstrated by soaking disposable filter paper in HOCOF solution and exposing them to NH_3. A visual color change from yellow to brownish red was observed in visible light along with a decrease in fluorescence emission under 365 nm UV light [Fig. 16C], indicating the potential of the sensor as an effective and economical strategy for the monitoring of ammonia in industrial production.

5. Azines as imaging agents

Since the discovery of the AIE phenomenon, the use of AIEgens for wash-free fluorescence detection and bioimaging has been attracting a lot of research attention.[119] However, AIE-active azines are occasionally used as imaging agents. Among one such study, Tharmalingam *et al.* reported an AIE-active unsymmetrical azine, **62**, by simple condensation of ethyl-α-cyano-5-formyl-2-pyrroleacrylate and 1-(hydrazonomethyl)naphthalene-2-ol and used it for the detection of Cu^{2+} ions.[120] The red-emissive azine was further utilized for practical application in imaging latent fingerprints (LFPs). LFPs were demonstrated by accumulating the thumb impressions on the TLC plate surface and coated with the aggregated mixture of **62** in DMSO containing 60% water. The removal of the excess solution of **62** and washing with water developed the latent fingerprints when exposed to 365 nm UV light [Fig. 17A]. Next, the imaging was demonstrated over different surfaces such as a glass TLC slide, aluminium foil, cello tape, currency paper, stainless slide and marble slate which showed that regardless of the surface material, the solid-phase fluorescence is achieved with significant intensity outputs [Fig. 17B].

The accumulation of β-amyloid (Aβ) in the brain is a pathological biomarker of Alzheimer's disease (AD), manifesting years prior to the appearance of symptoms, and its identification is an integral part of clinical diagnosis.[121] Li *et al.* demonstrated a class of diaryl-azines for detecting Aβ plaques in the AD brain using PET imaging.[122] They developed an Aβ-PET tracer, **63**, with a high binding affinity to the Aβ aggregates, significant binding ability with the AD brain sections, and optimal brain pharmacokinetic properties in rodents and non-human primates [Fig. 17C and D]. Dynamic PET studies of **63** demonstrated high initial brain uptake in APP/PS1 and WT mice, and subsequent clearance of the radiotracers from the brain was rapid [Fig. 17C]. An *in vivo* PET study in a rhesus monkey, devoid of Aβ pathology, suggested that **63** efficiently crossed the blood–brain barrier and accumulated in the cortex within 10 min, while rapidly decreasing the radioactivity to the baseline within 50 min [Fig. 17D]. Furthermore, the investigation of the overall body confirmed that no radio-defluorination takes place and **63** was highly stable in primates. The first-in-human PET study declared that **63** displayed low white matter uptake and could bind to Aβ pathology for distinguishing AD from healthy control subjects. The specific signal intensifications of **63** in the AD patient's cortex, especially in the frontal lobe and temporal lobe (common Aβ-burden regions), were confirmed [Fig. 17E]. Interestingly, the cortex of the HC subject did not show any presence of the relevant radioactivity retention and only a few signals were predominantly concentrated in the sub-cortical white matter.

6. Conclusion

Ever since the inception of the concept of aggregation-induced emission (AIE) in 2001, a new realm of research has unfolded, focusing on luminogenic molecules and materials based on their aggregation properties. Among various AIE-active systems, azines because of their easy synthesis and the ability to tune their luminescence emission through structural modifications are stand out performers with a range of practical applications. The introduction of bulky aromatic substituents and hindering intramolecular rotation through methods like metal chelation and hydrogen bonding can endow azines with AIE features. This review highlights the rationale behind the molecular design of azines and their tunable photophysical properties depending upon the substituents present on the aromatic scaffolds across the azine linkage. To date, many of these azines are derived from salicylaldehyde derivatives with fluorescence in the green to yellow region and are symmetrical across the azine bond. However, the condensation of two different aromatic aldehydes leads to unsymmetrical azines and although rarely documented, red to NIR emission can be achieved by proper tuning of the structure. The review primarily provides a comprehensive overview of the advancements in the realm of AIE-active azine molecules as chemosensors in detecting a diverse range of analytes emphasizing the developments in the last five years. It meticulously discusses the progress in various strategies employed for the detection of metal ions (Cu^{2+}, Zn^{2+}, Al^{3+}, Fe^{3+}, Cr^{3+}, Th^{4+}, Hg^{2+}, Mo^{6+}, UO_2^{2+}), anions (F^-, CN^-, ClO^-, $ONOO^-$, HSO_3^-), small molecules (thiols, picric acid, hydrogen peroxide), and bio-analytes (diethylchlorophosphate, alkaline phosphatase, β-lactamase, neuraminidase) focusing on the sensing mechanism, analytical prowess, real sample analysis, *etc.* It also covers the utilization of azines as dual sensors and multi-analyte sensors. Furthermore, the review describes the developments of azines in supramolecular sensors and sensing materials such as polymers and COFs/MOFs with selected examples to give a wholesome view of AIE-active azines in chemo-/bio-sensing applications. In the end, a section is focused on the azines as imaging agents. From the above discussion, it is apparent that AIE-active azines have immense potential as efficient probes for diverse chemosensing applications as well as to serve as imaging agents. Till date, AIE-active azines for functional bioimaging and tracing are rarely cited. However, the presence of two aromatic scaffolds allows incorporation of multiple functionalities as per the desire to design various organelle targeted AIE-azines. As a future perspective, water-soluble NIR or red-emissive azines with low cytotoxicity and better cell-permeability may be devised with the scope for biomedical and theragnostic applications

with a focus on organelle targeting and brain and neuron imaging.

Author contributions

Writing of review manuscript, drawing of ChemDraw structures, all figures, A. A. B.; the inception of the concept, planning the template, writing, and reviewing, M. B.; the inception of the concept and reviewing, A. C.

Conflicts of interest

The authors declare no competing financial interest.

Acknowledgements

A. A. B. is indebted to BITS Pilani University for institute-fellowship for SRF.

References

1 (*a*) J. Safari and S. Gandomi-Ravandi, *RSC Adv.*, 2014, **4**, 46224–46249; (*b*) T. Curtius and K. Thun, *J. Prakt. Chem.*, 1891, **44**, 161–186; (*c*) J.-P. Schirmann and P. Bourdauducq, in *Ullmann's Encyclopedia of Industrial Chemistry*, Wiley-VCH Verlag GmbH & Co. KGaA, Weinheim, Germany, 2001; (*d*) J. O. Bauer, G. Leitus, Y. Ben-David and D. Milstein, *ACS Catal.*, 2016, **6**, 8415–8419; (*e*) G. Moss, P. Smith and D. Tavernier, *Pure Appl. Chem.*, 1995, **67**, 1307–1375; (*f*) A. Ramakrishnan, S. S. Chourasiya and P. V. Bharatam, *RSC Adv.*, 2015, **5**, 55938–55947.

2 S. S. Chourasiya, D. Kathuria, A. A. Wani and P. V. Bharatam, *Org. Biomol. Chem.*, 2019, **17**, 8486–8521.

3 S. Kagatikar and D. Sunil, *J. Mol. Liq.*, 2019, **292**, 111371.

4 (*a*) M. Godara, R. Maheshwari, S. Varshney and A. K. Varshney, *J. Serb. Chem. Soc.*, 2007, **72**, 368–374; (*b*) A. I. Khodair and P. Bertrand, *Tetrahedron*, 1998, **54**, 4859–4872; (*c*) M. Chandra, A. N. Sahay, D. S. Pandey, R. P. Tripathi, J. K. Saxena, V. J. M. Reddy, M. C. Puerta and P. Valerga, *J. Organomet. Chem.*, 2004, **689**, 2256–2267; (*d*) J. Granifo, M. E. Vargas, E. S. Dodsworth, D. H. Farrar, S. S. Fielder and A. B. P. Lever, *J. Chem. Soc., Dalton Trans.*, 1996, 4369–4378; (*e*) A. Facchetti, A. Abbotto, L. Beverina, M. E. van der Boom, P. Dutta, G. Evmenenko, T. J. Marks and G. A. Pagani, *Chem. Mater.*, 2002, **14**, 4996–5005; (*f*) G. H. Brown and W. G. Shaw, *Chem. Rev.*, 1957, **57**, 1049–1157; (*g*) N. Mukherjee, C. Sun, B. Marie, S. Jin and R. M. Peetz, *Tetrahedron Lett.*, 2008, **49**, 1037–1040; (*h*) C. Amari, C. Pelizzi, G. Predieri, S. Destri and W. Porzio, *Synth. Met.*, 1995, **72**, 7–12; (*i*) H. S. Nalwa, T. Hamada and A. Kakuta, *Synth. Met.*, 1993, **57**, 3901–3906; (*j*) W. Hong, B. Sun, H. Aziz, W. T. Park, Y. Y. Noh and Y. Li, *Chem. Commun.*, 2012, **48**, 8413–8415; (*k*) J. J. Tindale, H. Holm, M. S. Workentin and O. A. Semenikhin, *J. Electroanal. Chem.*, 2008, **612**, 219–230.

5 *Photophysics of Aromatic Molecules*, ed. J. B. Birks, Wiley InterScience, London, 1970.

6 T. Förster and K. Kasper, *Z. Elektrochem.*, 1955, **59**, 976–980.

7 (*a*) J. Luo, Z. Xie, J. W. Y. Lam, L. Cheng, H. Chen, C. Qiu, H. S. Kwok, X. Zhan, Y. Liu, D. Zhuc and B. Z. Tang, *Chem. Commun.*, 2001, 1740–1741; (*b*) B. Z. Tang, X. Zhan, G. Yu, P. P. S. Lee, Y. Liu and D. Zhu, *J. Mater. Chem.*, 2001, **11**, 2974–2978.

8 (*a*) Y. Hong, J. W. Y. Lam and B. Z. Tang, *Chem. Soc. Rev.*, 2011, **40**, 5361–5388; (*b*) J. Mei, Y. Hong, J. W. Y. Lam, A. Qin, Y. Tang and B. Z. Tang, *Adv. Mater.*, 2014, **26**, 5429–5479; (*c*) Q. Xia, Y. Zhang, Y. Li, Y. Li, Y. Li, Z. Feng, X. Fan, J. Qian and H. Lin, *Aggregate*, 2022, **3**, e152; (*d*) J. Mei, N. L. C. Leung, R. T. K. Kwok, J. W. Y. Lam and B. Z. Tang, *Chem. Rev.*, 2015, **115**, 11718–11940; (*e*) H. Wang, E. Zhao, J. W. Y. Lam and B. Z. Tang, *Mater. Today*, 2015, **18**, 365–377; (*f*) G. R. Suman, M. Pandey and A. S. J. Chakravarthy, *Mater. Chem. Front.*, 2021, **5**, 1541–1584; (*g*) Z. He, C. Ke and B. Z. Tang, *ACS Omega*, 2018, **3**, 3267–3277; (*h*) R. T. K. Kwok, C. W. T. Leung, J. W. Y. Lam and B. Z. Tang, *Chem. Soc. Rev.*, 2015, **44**, 4228–4238; (*i*) Y. Hong, J. W. Y. Lam and B. Z. Tang, *Chem. Commun.*, 2009, 4332–4353; (*j*) D. Ding, K. Li, B. Liu and B. Z. Tang, *Acc. Chem. Res.*, 2013, **46**, 2441–2453.

9 S. Poojary, D. Sunil, D. Kekuda and S. Sreenivasa, *Opt. Mater.*, 2018, **85**, 1–7.

10 T. Zheng, J.-L. Xu, X.-J. Wang, J. Zhang, X. Jiao, T. Wang and D. Chen, *Chem. Commun.*, 2016, **52**, 6922–6925.

11 S. Kagatikar, D. Sunil, D. Kekuda, S. D. Kulkarni and A. A. A. Salam, *J. Mol. Liq.*, 2020, **318**, 114029.

12 T. Mondal, S. Roy, I. Mondal, M. V. Mane and S. S. Panja, *J. Photochem. Photobiol., A*, 2021, **406**, 112998.

13 P. Acker, M. E. Speer, J. S. Wössner and B. Esser, *J. Mater. Chem. A*, 2020, **8**, 11195–11201.

14 D. Liu, K. Li, M. Li, Z. Wang, M. Shan and Y. Zhang, *ACS Appl. Mater. Interfaces*, 2021, **13**, 37775–37784.

15 S. Bondock, T. Albarqi, I. A. Shaaban and M. M. Abdou, *RSC Adv.*, 2023, **13**, 10353–10366.

16 S. Kaide, H. Watanabe, Y. Shimizu, S. Iikuni, Y. Nakamoto, M. Hasegawa, K. Itoh and M. Ono, *ACS Chem. Neurosci.*, 2020, **11**, 4254–4261.

17 S. Biswas, R. Mengji, S. Barman, V. Venugopal, A. Jana and N. D. P. Singh, *Chem. Commun.*, 2018, **54**, 168–171.

18 J.-L. Xu, Y. Quan, Q.-Y. Li, H. Lu, H. Wu, J. Yin, X.-J. Wang and Q. Zhang, *RSC Adv.*, 2015, **5**, 88176–88180.

19 S. Guo, Y. Song, Y. He, X.-Y. Hu and L. Wang, *Angew. Chem., Int. Ed.*, 2018, **57**, 3163–3167.

20 W. Tang, Y. Xiang and A. Tong, *J. Org. Chem.*, 2009, **74**, 2163–2166.

21 X. Chen, Y. Xiang, P. Song and A. Tong, *Analyst*, 2010, **135**, 1098–1105.

22 L. Peng, Z. Zhou, X. Wang, R. Wei, K. Li, Y. Xiang and A. Tong, *Anal. Chim. Acta*, 2014, **829**, 54–59.

23 Z. Li, Y. Zhang, H. Xia, Y. Mua and X. Liu, *Chem. Commun.*, 2016, **52**, 6613–6616.

24 N. Gupta, T. Kaur, V. Bhalla, R. D. Parihar, P. Ohri, G. Kaur and M. Kumar, *Chem. Commun.*, 2017, **53**, 12646–12649.

25 Y. Zhao, Y. Li, Y. Long, Z. Zhou, Z. Tang, K. Deng and S. Zhang, *Tetrahedron Lett.*, 2017, **58**, 1351–1355.
26 Y.-H. Zhao, Y. Luo, H. Wang, T. Guo, H. Zhou, H. Tan, Z. Zhou, Y. Long and Z. Tang, *ChemistrySelect*, 2018, **3**, 1521–1526.
27 H. L. Nguyen, N. Kumar, J.-F. Audibert, R. Ghasemi, J.-P. Lefevre, M.-H. Ha-Thi, C. Mongin and I. Leray, *New J. Chem.*, 2019, **43**, 15302–15310.
28 S. Manigandan, A. Muthusamy, R. Nandhakumar and C. I. David, *J. Mol. Struct.*, 2020, **1208**, 127834.
29 A. A. Bhosle, S. D. Hiremath, A. C. Bhasikuttan, M. Banerjee and A. Chatterjee, *J. Photochem. Photobiol., A*, 2021, **413**, 113265.
30 A. A. Bhosle, M. Banerjee, S. Saha, S. Garg, S. Ghosh and A. Chatterjee, *Sens. Actuators, B*, 2023, **397**, 134661.
31 X. Chen, R. Wei, Y. Xiang, Z. Zhou, K. Li, P. Song and A. Tong, *J. Phys. Chem. C*, 2011, **115**, 14353–14359.
32 R. Wei, P. Song and A. Tong, *J. Phys. Chem. C*, 2013, **117**, 3467–3474.
33 X. Yao, J.-X. Ru, C. Xu, Y.-M. Liu, W. Dou, X.-L. Tang, G.-L. Zhang and W.-S. Liu, *ChemistryOpen*, 2015, **4**, 478–482.
34 S. Samanta, U. Manna and G. Das, *New J. Chem.*, 2017, **41**, 1064–1072.
35 M. Mathivanan, B. Tharmalingam, C.-H. Lin, B. V. Pandiyan, V. Thiagarajan and B. Murugesapandian, *CrystEngComm*, 2020, **22**, 213–228.
36 M. Mathivanan and B. Murugesapandian, *Dyes Pigm.*, 2022, **203**, 110367.
37 A. A. Bhosle, M. Banerjee, S. D. Hiremath, A. C. Bhasikuttan and A. Chatterjee, *Chem. – Asian J.*, 2023, **18**, e202300048.
38 M. K. Dixit and M. Dubey, *Phys. Chem. Chem. Phys.*, 2018, **20**, 23762–23772.
39 D. H. Brown and W. E. Smith, Metal ions in biological systems, in *Enzyme Chemistry*, ed. C. J. Suckling, Springer, Dordrecht, 1984, DOI: **10.1007/978-94-009-5574-5_6**.
40 (*a*) X. Zheng, W. Cheng, C. Ji, J. Zhang and M. Yin, *Rev. Anal. Chem.*, 2020, **39**, 231–246; (*b*) Y. Shi, W. Zhang, Y. Xue and J. Zhang, *Chemosensors*, 2023, **11**, 226.
41 A. K. Saini, K. Natarajan and S. M. Mobin, *Chem. Commun.*, 2017, **53**, 9870–9873.
42 J.-H. Hu, Y. Sun, J. Qi, Q. Li and T.-B. Wei, *Spectrochim. Acta, Part A*, 2017, **175**, 125–133.
43 A. Ghosh, S. Adhikari, S. Ta, A. Banik, T. K. Dangar, S. K. Mukhopadhyay, J. S. Matalobos, P. Brandão, V. Félix and D. Das, *Dalton Trans.*, 2016, **45**, 19491–19499.
44 X. Chen, L. He, Y. Wang, B. Liu and Y. Tang, *Anal. Chim. Acta*, 2014, **847**, 55–60.
45 X. Chen, L. Peng, M. Feng, Y. Xiang, A. Tong, L. He, B. Liu and Y. Tang, *J. Lumin.*, 2017, **186**, 301–306.
46 H. Zhou, B. Yang, G. Wen, X. Hu and B. Liu, *Talanta*, 2018, **184**, 394–403.
47 B. Tharmalingam, M. Mathivanan, G. Dhamodiran, K. S. Mani, M. Paranjothy and B. Murugesapandian, *ACS Omega*, 2019, **4**, 12459–12469.
48 K. Tiwari, S. Kumar, V. Kumar, J. Kaur, S. Arora and R. K. Mahajan, *Spectrochim. Acta, Part A*, 2018, **191**, 16–26.
49 W. Ye, M. Xie, J. Wei, G. Li, Y. Tang, L. Hou, L. Wang, H. Yu, C.-S. Lee and H. Xu, *Sens. Actuators, B*, 2021, **343**, 130106.
50 J. Liu, C. Leng, Q. Chen, Q. Liang, C. Li, S. Li, Z. Zhang and L. Xiao, *ChemistrySelect*, 2022, **7**, e202203313.
51 K. Kumarasamy, T. Devendhiran, M.-C. Lin, W.-J. Chien, S. K. Ramasamy, S. Manickam and J.-C. Yang, *Inorg. Chem. Commun.*, 2022, **145**, 110020.
52 S. Sharifi, A. W. Mesbah and E. Iravani, *Results Chem.*, 2023, **5**, 100747.
53 G. Kumar, K. Paul and V. Luxami, *Sens. Actuators, B*, 2018, **263**, 585–593.
54 S. Khanra, S. Ta, M. Ghosh, S. Chatterjee, P. Mukherjee and D. Das, *New J. Chem.*, 2020, **44**, 8477–8485.
55 S. Khanra, S. Ta, M. Ghosh, S. Chatterjee and D. Das, *RSC Adv.*, 2019, **9**, 21302–21310.
56 B. Das, M. Dolai, A. Dhara, S. Mabhai, A. Jana, S. Dey and A. Misra, *Anal. Sci. Adv.*, 2021, **2**, 447–463.
57 B. Musikavanhu, Y. Zhang, D. Zhu, Z. Xue, R. Yuan, S. Wang and L. Zhao, *Spectrochim. Acta, Part A*, 2022, **281**, 121599.
58 T. Mondal, I. Mondal, S. Biswas, M. V. Mane and S. S. Panja, *ChemistrySelect*, 2020, **5**, 9336–9349.
59 J. Tong, K. Zhang, J. Wang, H. Li, F. Zhou, Z. Wang, X. Zhang and B. Z. Tang, *J. Mater. Chem. C*, 2020, **8**, 996–1001.
60 M. Ghosh, S. Ta, J. S. Matalobos and D. Das, *Dalton Trans.*, 2018, **47**, 11084–11090.
61 X.-Q. Pham, N. Kumar, M.-H. Ha-Thi and I. Leray, *J. Photochem. Photobiol., A*, 2019, **373**, 139–145.
62 R. Yadav, A. Rai, A. K. Sonkar, V. Rai, S. C. Gupta and L. Mishra, *New J. Chem.*, 2019, **43**, 7109–7119.
63 X.-M. Sun, J. Liu, Z.-H. Li, Y.-P. Fu, T.-T. Huang, Z.-D. Tang, B. Shi, H. Yao, T.-B. Wei and Q. Lin, *Chin. Chem. Lett.*, 2023, **34**, 107792.
64 B. Das, M. Dolai, A. Dhara, A. Ghosh, S. Mabhai, A. Misra, S. Dey and A. Jana, *J. Phys. Chem. A*, 2021, **125**, 1490–1504.
65 M. Dolai, U. Saha, A. K. Das and G. S. Kumar, *Anal. Methods*, 2018, **10**, 4063–4072.
66 S. Sawminathan, S. Munusamy, S. Manickam, D. Jothi and S. KulathuIyer, *Dyes Pigm.*, 2021, **196**, 109755.
67 N. Kaur, G. Kaur, U. A. Fegade, A. Singh, S. K. Sahoo, A. S. Kuwar and N. Singh, *TrAC, Trends Anal. Chem.*, 2017, **95**, 86–109.
68 (*a*) J. F. Zhang, C. S. Lim, S. Bhuniya, B. R. Cho and J. S. Kim, *Org. Lett.*, 2011, **13**, 1190–1193; (*b*) P. Pacher, J. S. Beckman and L. Liaudet, *Physiol. Rev.*, 2007, **87**, 315–424; (*c*) F. Wang, L. Wang, X. Chen and J. Yoon, *Chem. Soc. Rev.*, 2014, **43**, 4312–4324; (*d*) B. Pan, H. Ren, X. Lv, Y. Zhao, B. Yu, Y. He, Y. Ma, C. Niu, J. Kong, F. Yu, W. Sun, Y. Zhang, B. Willard and L. Zheng, *J. Transl. Med.*, 2012, **10**, 65; (*e*) A. F. Gunnison, D. W. Jacobsen and H. J. Schwartz, *Crit. Rev. Toxicol.*, 1987, **17**, 185–214.
69 B. Yu, C.-Y. Li, Y.-X. Sun, H.-R. Jia, J.-Q. Guo and J. Li, *Spectrochim. Acta, Part A*, 2017, **184**, 249–254.
70 P.-X. Pei, J.-H. Hu, Y. Chen, Y. Sun and J. Qi, *Spectrochim. Acta, Part A*, 2017, **181**, 131–136.

71 Y. Sun, J.-H. Hu, J. Qi and J.-B. Li, *Spectrochim. Acta, Part A*, 2016, **167**, 101–105.
72 J. Yang, J. Rui, X. Xu, Y. Yang, J. Su, H. Xu, Y. Wang, N. Sun and S. Wang, *RSC Adv.*, 2016, **6**, 30636–30641.
73 Y. Shen, M. Li, M. Yang, Y. Zhang, H. Li and X. Zhang, *Spectrochim. Acta, Part A*, 2019, **222**, 117230.
74 X. Yuan, C.-X. Zhao, Y.-X. Lu, Y.-J. Shen and C.-Y. Wang, *J. Photochem. Photobiol., A*, 2018, **361**, 41–47.
75 T. Devendhiran, K. Kumarasamy, M.-C. Lin and Y. X. Yang, *Inorg. Chem. Commun.*, 2021, **134**, 108951.
76 Y. Yao, X.-M. Fu and J.-H. Hu, *Inorg. Chem. Commun.*, 2022, **141**, 109557.
77 S. Paul, K. Debsharma, S. Dey, S. Halder, K. Jana and C. Sinha, *Mater. Adv.*, 2023, **4**, 3874–3891.
78 G. Singh, A. Kaur, M. Sharma, V. Bhalla, D. Singh, S. Arora and M. Kumar, *Mater. Adv.*, 2020, **1**, 1347–1353.
79 (*a*) J. R. Burgoyne, S. I. Oka, N. Ale-Agha and P. Eaton, *Antioxid. Redox Signaling*, 2013, **18**, 1042–1052; (*b*) S. Garrod, M. E. Bollard, A. W. Nicholls, S. C. Connor, J. Connelly, J. K. Nicholson and E. Holmes, *Chem. Res. Toxicol.*, 2005, **18**, 115–122; (*c*) G. J. Despotis, G. Gravlee, K. Filos, J. Levy and D. M. Fisher, *Anesthesiology*, 1999, **91**, 1122–1151; (*d*) Q. Shao, Y. Zheng, X. Dong, K. Tang, X. Yan and B. Xing, *Chem. – Eur. J.*, 2013, **19**, 10903–10910; (*e*) G. M. Air and W. G. Laver, *Proteins: Struct., Funct., Bioinf.*, 1989, **6**, 341–356; (*f*) Y. Zhou and J. Yoon, *Chem. Soc. Rev.*, 2012, **41**, 52–67.
80 L. Peng, Z. Zhou, R. Wei, K. Li, P. Song and A. Tong, *Dyes Pigm.*, 2014, **108**, 24–31.
81 H. Liu, P. Song, R. Wei, K. Li and A. Tong, *Talanta*, 2014, **118**, 348–352.
82 L. Peng, R. Wei, K. Li, Z. Zhou, P. Song and A. Tong, *Analyst*, 2013, **138**, 2068–2072.
83 X.-T. Chen, Y. Xiang and A. J. Tong, *Talanta*, 2010, **80**, 1952–1958.
84 X.-T. Chen and A. J. Tong, *J. Lumin.*, 2014, **145**, 737–740.
85 M. Gao, C. K. Sim, C. W. T. Leung, Q. Hu, G. Feng, F. Xu, B. Z. Tang and B. Liu, *Chem. Commun.*, 2014, **50**, 8312–8315.
86 L. Peng, M. Gao, X. Cai, R. Zhang, K. Li, G. Feng, A. Tong and B. Liu, *J. Mater. Chem. B*, 2015, **3**, 9168–9172.
87 H. Liu, R. Wei, Y. Xiang and A. Tong, *Anal. Methods*, 2015, **7**, 753–758.
88 X. Ma, J. Cheng, J. Liu, X. Zhou and H. Xiang, *New J. Chem.*, 2015, **39**, 492–500.
89 M. Sathiyaraj, K. Pavithra and V. Thiagarajan, *New J. Chem.*, 2020, **44**, 8402–8411.
90 A. A. Bhosle, M. Banerjee, V. Gupta, S. Ghosh, A. C. Bhasikuttan and A. Chatterjee, *New J. Chem.*, 2022, **46**, 18961–18972.
91 H. Song, Y. Zhou, H. Qu, C. Xu, X. Wang, X. Liu, Q. Zhang and X. Peng, *Ind. Eng. Chem. Res.*, 2018, **57**, 15216–15223.
92 M. Bhattu, A. A. Wani, M. Verma, P. V. Bharatam, D. Kathuria and J. Simal-Gandara, *J. Photochem. Photobiol., A*, 2023, **437**, 114476.
93 R. Suhasini, R. Karpagam, K. Thirumoorthy and V. Thiagarajan, *Spectrochim. Acta, Part A*, 2021, **263**, 120206.
94 M. Sathiyaraj and V. Thiagarajan, *RSC Adv.*, 2020, **10**, 25848–25855.
95 Y. He, J. Yu, X. Hu, S. Huang, L. Cai, L. Yang, H. Zhang, Y. Jiang, Y. Jia and H. Sun, *Chem. Commun.*, 2020, **56**, 13323–13326.
96 L. Peng, L. Xiao, Y. Ding, Y. Xiang and A. Tong, *J. Mater. Chem. B*, 2018, **6**, 3922–3926.
97 H. Chang, Y. Mei, Y. Li and L. Shang, *Talanta*, 2022, **247**, 123583.
98 (*a*) S. Mukhopadhyay, R. K. Gupta, A. Biswas, A. Kumar, M. Dubey, M. S. Hundal and D. S. Pandey, *Dalton Trans.*, 2015, **44**, 7118–7122; (*b*) Y. Liang, R. Wang, G. Liu and S. Pu, *ACS Omega*, 2019, **4**, 6597–6606; (*c*) X. He, J. Zhang, X. Liu, L. Dong, D. Li, H. Qiu and S. Yin, *Sens. Actuators, B*, 2014, **192**, 29–35; (*d*) L. Wang, X. Gong, Q. Bing and G. Wang, *Microchem. J.*, 2018, **142**, 279–287.
99 P. Yadav, S. Gond, A. Shekher, S. C. Gupta, U. P. Singh and V. P. Singh, *Dalton Trans.*, 2022, **51**, 6927–6935.
100 (*a*) T. L. Mako, J. M. Racicot and M. Levine, *Chem. Rev.*, 2019, **119**, 322–477; (*b*) S. Lim, Y. Kuang and H. A. M. Ardoña, *Front. Chem.*, 2021, **9**, 723111.
101 (*a*) M. Huo, Q. Ye, H. Che, X. Wang, Y. Wei and J. Yuan, *Macromolecules*, 2017, **50**, 1126–1133; (*b*) Z. Zhang, Y. Lou, C. Guo, Q. Jia, Y. Song, J.-Y. Tian, S. Zhang, M. Wang, L. He and M. Du, *Trends Food Sci. Technol.*, 2021, **118**, 569–588; (*c*) Y. Yue, D. Ji, Y. Liu and D. Wei, *Chem. – Eur. J.*, 2023, e202302474.
102 (*a*) A. A. Bhosle, M. Banerjee, N. Barooah, A. C. Bhasikuttan, K. Kadu, S. R. Ramanan and A. Chatterjee, *J. Photochem. Photobiol., A*, 2022, **426**, 113770; (*b*) A. A. Bhosle, M. Banerjee, S. D. Hiremath, D. S. Sisodiya, V. G. Naik, N. Barooah, A. C. Bhasikuttan, A. Chattopadhyay and A. Chatterjee, *J. Mater. Chem. B*, 2022, **10**, 8258–8273.
103 V. Ganesan, M. K. Mani, V. Narayanan, E. Shanmugasundram, K. Vellaisamy, V. Baskaralingam, J. Jeyaraj, G. B. Veerakanellore, R. Rajamohan and S. Thambusamy, *J. Photochem. Photobiol., A*, 2023, **442**, 114814.
104 V. Narayanan, V. Ganesan, E. Shanmugasundram, S. Durganandini, K. Vellaisamy, H. Amirthalingam, R. Rajamohan and S. Thambusamy, *J. Photochem. Photobiol., A*, 2023, **445**, 115069.
105 (*a*) Z. Qiu, X. Liu, J. W. Y. Lam and B. Z. Tang, *Macromol. Rapid Commun.*, 2019, **40**, 1800568; (*b*) R. Hu, D. Xin, A. Qin and B. Z. Tang, *Acta Polym. Sin.*, 2018, **2**, 132–144; (*c*) H. Chen, E. Zhang, G. Yang, L. Li, L. Wu, Y. Zhang, Y. Liu, G. Chen and M. Jiang, *ACS Macro Lett.*, 2019, **8**, 893–898; (*d*) K. Morishima, F. Ishiwari, S. Matsumura, T. Fukushima and M. Shibayama, *Macromolecules*, 2017, **50**, 5940–5945.
106 (*a*) M. Huo, Q. Ye, H. Che, X. Wang, Y. Wei and J. Yuan, *Macromolecules*, 2017, **50**, 1126–1133; (*b*) Y. Wu, L. Qu, J. Li, L. Huang and Z. Liu, *Polymer*, 2018, **158**, 297–307; (*c*) Y. Li, F. Gao, J. Guo, P. Ren, Z. Tian, J. Bai and J. Hua, *Eur. Polym. J.*, 2020, **122**, 109355.
107 J. Huang, H. Qin, H. Liang and J. Lu, *Polymers*, 2020, **202**, 122663.

108 H. Qin, J. Huang, H. Liang and J. Lu, *ACS Appl. Mater. Interfaces*, 2021, **13**, 5668–5677.
109 W. Liang, D. Liu, J. Huang, H. Liang and J. Lu, *Dyes Pigm.*, 2022, **200**, 110115.
110 P. Wang, B. Liang and D. Xi, *Inorg. Chem.*, 2019, **58**, 2252–2256.
111 (*a*) R. W. Flaig, T. M. Osborn Popp, A. M. Fracaroli, E. A. Kapustin, M. J. Kalmutzki, R. M. Altamimi, F. Fathieh, J. A. Reimer and O. M. Yaghi, *J. Am. Chem. Soc.*, 2017, **139**, 12125–12128; (*b*) M. Tanhaei, A. R. Mahjoub and V. Safarifard, *Mater. Lett.*, 2018, **227**, 318–321.
112 (*a*) Y. Zhang, S. Yuan, G. Day, X. Wang, X. Yan and H.-C. Zhou, *Coord. Chem. Rev.*, 2017, **354**, 28–45; (*b*) Z. Hu, B. J. Deibert and J. Li, *Chem. Soc. Rev.*, 2014, **43**, 5815–5840.
113 Y. D. Farahani and V. Safarifard, *J. Solid State Chem.*, 2019, **270**, 428–435.
114 D. Mukherjee, A. Pal, S. C. Pal, A. Saha and M. C. Das, *Inorg. Chem.*, 2022, **61**, 16952–16962.
115 M. Kaur, M. Yusuf and A. K. Malik, *J. Fluoresc.*, 2023, **33**, 339–357.
116 X. Feng, X. Ding and D. Jiang, *Chem. Soc. Rev.*, 2012, **41**, 6010–6022.
117 R. K. Sharma, P. Yadav, M. Yadav, R. Gupta, P. Rana, A. Srivastava, R. Zbořil, R. S. Varma, M. Antonietti and M. B. Gawande, *Mater. Horiz.*, 2020, **7**, 411–454.
118 Y.-D. Xia, Y. Cheng, Y.-J. Wu, Y. Xia and X.-B. Yin, *Chem. Mater.*, 2023, **35**, 2579–2587.
119 (*a*) J. Qian and B. Z. Tang, *Chem*, 2017, **3**, 56–91; (*b*) X. Huang, R. Zhang, C. Chen, R. T. K. Kwok and B. Z. Tang, *Mater. Chem. Front.*, 2021, **5**, 723–743; (*c*) Y. Chen, *Mater. Today Chem.*, 2022, **25**, 100975; (*d*) S. Wang, K. Zhou, X. Lyu, H. Li, Z. Qiu, Z. Zhao and B. Z. Tang, *Chem. Biomed. Imaging*, 2023, **1**, 509–521.
120 B. Tharmalingam, O. Anitha, J. Aiswarya, T. Thiruppathiraja, S. Lakshmipathi and B. Murugesapandian, *J. Photochem. Photobiol., A*, 2023, **442**, 114757.
121 V. L. Villemagne, S. Burnham, P. Bourgeat, B. Brown, K. A. Ellis, O. Salvado, C. Szoeke, S. L. Macaulay, R. Martins, P. Maruff, D. Ames, C. C. Rowe and C. L. Masters, *Lancet Neurol.*, 2013, **12**, 357–367.
122 Y. Li, K. Zhou, X. Zhang, H. Zhao, X. Wang, R. Dong, Y. Wang, B. Chen, X.-x. Yan, J. Dai, Y. Sui, J. Zhang and M. Cui, *J. Med. Chem.*, 2023, **66**, 4603–4616.